iScience

Article

Deciphering the anti-obesity mechanisms of pharmabiotic probiotics through advanced multiomics analysis

Graphical abstract

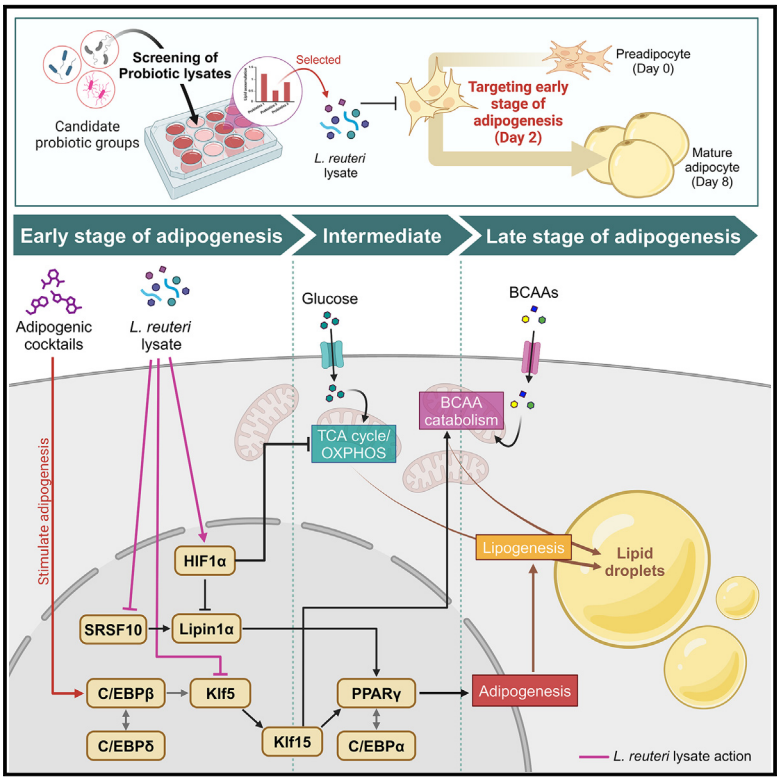

Highlights

- *L. reuteri* lysate suppresses adipocyte differentiation during early adipogenesis
- *L. reuteri* lysate inhibits KLF5 and reduces PPARγ expression and BCAA catabolism
- *L. reuteri* lysate induces metabolic changes via HIF1α and regulates lipin-1 isoform
- KLF5 and HIF1α mediate *L. reuteri* lysate's inhibitory effects on adipogenesis

Authors

Ye-Rim Kim, Tae-Rim Choi, Sung-Hyun Jo, ..., Chol-Soon Jang, Yung-Hun Yang, Yun-Gon Kim

Correspondence

ygkim@ssu.ac.kr

In brief

Obesity medicine; Microbiology; Microbiome; Omics

Kim et al., 2025, iScience *28*, 111890
February 21, 2025
https://doi.org/10.1016/j.isci.2025.111890

CellPress

iScience

CellPress
OPEN ACCESS

Article

Deciphering the anti-obesity mechanisms of pharmabiotic probiotics through advanced multiomics analysis

Ye-Rim Kim,[1] Tae-Rim Choi,[2] Sung-Hyun Jo,[1] Won-Suk Song,[3] TaeHyun Kim,[4] Min-Gyu Kim,[1] Ji-Hyun Baek,[1] Seo-Young Kwon,[1] Bo-Gyeong Choi,[1] Sang Woo Seo,[4] Chol-Soon Jang,[4] Yung-Hun Yang,[2] and Yun-Gon Kim[1,5,*]

[1]Department of Chemical Engineering, Soongsil University, Seoul 06978, Republic of Korea
[2]Department of Biological Engineering, College of Engineering, Konkuk University, Seoul 05029, Republic of Korea
[3]Department of Biological Chemistry, University of California, Irvine, Irvine, CA 92697, USA
[4]School of Chemical and Biological Engineering, Seoul National University, Seoul 08826, Republic of Korea
[5]Lead contact
*Correspondence: ygkim@ssu.ac.kr
https://doi.org/10.1016/j.isci.2025.111890

SUMMARY

Probiotics with "pharmabiotic" properties are increasingly recognized as effective tools for combating obesity by altering gut microbiota and reducing body fat. However, the molecular mechanisms underlying their anti-obesity effects remain largely unexplored due to the absence of a universal methodology. Herein, we developed a multiomics-based strategy to elucidate how probiotics reduce lipid production in adipocytes. Our initial investigation assessed the impact of probiotics at defined adipocyte differentiation stages. Leveraging these insights, we performed comprehensive multiomics analyses at key intervals to identify the suppression mechanisms of lipid formation. *Lactobacillus reuteri*, specifically, targets early differentiation stages, inhibits branched-chain amino acid catabolism, and reduces lipid accumulation in adipocytes by suppressing Krüppel-like factor 5. Concurrently, enhanced hypoxia-inducible factor 1 expression impedes adipogenesis by downregulating lipin-1 expression. This study not only demonstrates the effectiveness of our approach in revealing complex host-microbe interactions but also significantly advances probiotic therapeutic development, offering promising avenues for obesity management.

INTRODUCTION

Global obesity rates have almost doubled since 1980, with over one-third of the global population now overweight or obese, rendering obesity a major public health concern.[1] Obesity is defined as an abnormal or excessive accumulation of fat to the point of impairing health.[2] Excess fat stored in the body increases the risk of metabolic disorders, such as type 2 diabetes and cardiovascular diseases.[3] Lifestyle and environmental factors play a pivotal role in the current rapid increase in obesity prevalence despite the significant influence of genetic factors on obesity development.[4,5] The changes in the lifestyle of modern people, including diet and physical activity, ultimately lead to an imbalance in energy intake and expenditure, resulting in obesity.[6] Efforts to prevent obesity are being conducted in many countries, but for patients with obesity above a certain level, additional treatment, including drugs or surgery, may be required.[7] However, surgical intervention (e.g., bariatric surgery) alone is insufficient to meet the medical needs of the obese population. Thus, there is increasing interest in the development of anti-obesity medications (AOMs), which are expected to fulfill the unmet medical demands for obesity treatment. Despite many efforts to develop effective AOMs, safety concerns due to various side effects have prevented many treatments from being approved for use.[8] Therefore, appropriate drug candidates that are safe and effective for treating obesity are crucial for developing AOMs. In this perspective, probiotics, known to exert various positive effects on the host's energy balance and metabolism, are emerging as novel candidates for AOMs.

Probiotics are defined as live microorganisms that provide health benefits to the host when consumed in adequate amounts.[9] Recently, the concept has been expanded to include postbiotics, which have similar benefits to probiotics.[10] Probiotics generally affect host health by improving gut dysbiosis and modulating metabolism.[9,11] Gut dysbiosis can contribute to obesity through alterations in energy and lipid metabolisms.[12] Interest in developing probiotics as therapeutic adjuvants is increasing, offering promising pharmacotherapy to improve this condition.[13,14] *Lactobacillus* spp. and *Bifidobacterium* spp. are representative probiotics known for their safety profile and effectiveness on various diseases, including obesity, metabolic disorders, and immune disorders.[15] Several probiotics, including *Lactobacillus* spp. and *Bifidobacterium* spp., have been reported to exhibit anti-obesity effects *in vivo* or *in vitro*, and their potential as novel medications for obesity is attracting

attention.[16,17] Studies on the mechanism of action (MOA) of new disease treatments are important for validating and assessing their efficacy and predicting possible side effects.[18] Therefore, target identification and MOA studies at the molecular level are crucial for therapeutic probiotic research.[19] Nevertheless, identifying the exact mechanism is challenging due to the complexity of probiotics, which is more intricate than common drugs, and the complex regulation of adipocyte differentiation.[19,20] Despite the increasing number of reports on the anti-obesity effect of probiotics, research on the MOA for individual probiotics remains unclear.[21] To date, many studies have evaluated the anti-obesity effect of probiotics by analyzing single genes and proteins related to lipogenesis in adipocytes and adipose tissues. However, to fully recognize the anti-obesity characteristics of probiotics, it is essential to identify specific biomarkers and develop a method to confirm changes in metabolic pathways.[19–21] In this context, there is an increasing emphasis on using "multiomics" approaches to improve our molecular understanding of the complex MOA of probiotics by providing robust data.[21,22]

Despite extensive research regarding the multistep transcriptional complexity of adipocytes, attempts to analyze lipid suppression mechanisms focusing specifically on the timing of adipocyte differentiation have not always been successful.[23] Herein, we established an advanced multiomics workflow to identify the mechanisms inhibiting adipogenesis in adipocytes to assess the anti-obesity effect of a complex treatment including probiotics (Figure 1). First, adipocyte differentiation was categorized into early (days 0–2), intermediate (days 2–4), and late (days 4–8) stages based on changes in major transcription factors to determine the inhibitory effect on each stage. Subsequently, proteomics was performed on adipocytes at the stage where the inhibitory effect was observed, as well as on mature adipocytes to compare the changes in metabolic pathways. Based on the proteomics results, additional metabolomic and lipidomic analyses were performed to confirm the metabolic changes in adipocytes and predict the MOA, which was finally validated via mRNA expression analysis. As a model study, 15 species of probiotics were randomly prescreened from *Lactobacillus* spp. and *Bifidobacterium* spp., which are generally recognized as safe and previously reported for their antiadipogenic potential.[15] Among them, we selected *L. reuteri*, which most effectively inhibits adipocyte lipid accumulation, and identified its inhibition mechanism. Following the workflow presented in this study, *L. reuteri* was found to have a significant effect, particularly at the early stage of adipocyte differentiation. *L. reuteri* reduced lipid accumulation in adipocytes by inhibiting branched-chain amino acid (BCAA) catabolism, specifically targeting early differentiation. *L. reuteri* inhibited the expression of KLF5 during early adipocyte differentiation, resulting in the downregulation of PPARγ expression and reduction in BCAA catabolism. Simultaneously, *L. reuteri* inhibited adipogenesis by promoting the expression of HIF-1α and downregulating the expression of lipin-1 in early adipocyte differentiation. This discovery shows that our multiomics strategy can identify new mechanisms and target molecules for inhibiting adipogenesis through probiotics.

RESULTS AND DISCUSSION

Screening of bacterial strains and investigating the stages of adipocyte differentiation

To be recognized as bacterial strains with antiadipogenic potential, bacteria should be able to interfere with lipid accumulation in differentiated adipocytes without causing significant changes in the cell viability of adipocytes.[24] In our results, probiotic lysates except *L. johnsonii* inhibited lipid accumulation in 3T3-L1 adipocytes (Figure 2A), while *B. animalis* subsp. *animalis*, *B. longum*, *B. animalis* subsp. *Lactis*, and *B. bifidum* substantially damaged cells in the treatment process (Figure 2B). Among other strains, *L. fermentum* (48.56% in 5×10^7 colony-forming unit [CFU]/mL) and *L. reuteri* (54.11% in 5×10^7 CFU/mL) caused superior lipid accumulation inhibition at the same CFU concentration. Therefore, we considered *L. reuteri* (5×10^7 CFU/mL), which reduced lipid accumulation to the maximum extent compared to the control, as a model candidate for studying probiotics to validate the objectives of this study.

Some strains of *L. reuteri* have been consistently demonstrated in previous studies to exert anti-obesity effects by suppressing lipid accumulation in the liver or adipose tissue.[25–27] The anti-obesity effect of *L. reuteri* was observed *in vivo* or *in vitro* not only in live cells[25,26] but also in dead cells[26] or lysate derived from them.[27] Specifically, the reported strain in *L. reuteri* was identical to the *L. reuteri* strain tested in this study.[27] However, despite numerous reports on the anti-obesity properties of *L. reuteri* strains,[25–27] most studies have been based on phenotypic characteristics and have not provided a clear mechanism of how *L. reuteri* strains inhibit adipogenesis through metabolic processes. A study was conducted using a multiomics approach to evaluate the anti-obesity properties of *L. reuteri*, investigate its mechanism and molecular target in adipocytes, and address uncertainties found in previous studies.

Adipogenesis converts preadipocytes with fibroblast-like phenotype into adipocytes capable of accumulating lipids. This adipocyte differentiation process is highly regulated involving an intricate interaction of various metabolic pathways, and different stages of adipocyte differentiation result in different phenotypes.[28] Therefore, we divided adipocyte differentiation into three stages (early, intermediate, and late) and treated the aforementioned lysate of *L. reuteri* at each stage to identify the key steps involved in cell differentiation (Figure 3A). First, the treatment conditions of days 0–2, days 0–4, and days 0–8 showed a significant difference from the control and a reduction in lipid accumulation of about 40%, suggesting that *L. reuteri* showed antiadipogenic potential when treated at the early differentiation stage of days 0–2 (Figure 3B). In addition, when *L. reuteri* was treated only from days 0–2 by concentration, it showed a reduction in lipid accumulation of 54.4% (5×10^7 CFU/mL), which was similar to the results in Figure 2A, where treatment was administered from days 0–8 (Figure 3C). As adipogenesis progressed, adipocytes and lipid droplet size were significantly reduced compared to the control (Figure S1). Furthermore, image analysis using ImageJ confirmed a reduction in the lipid accumulation area of adipocytes by *L. reuteri* treatment, like previous results (Figure S2).

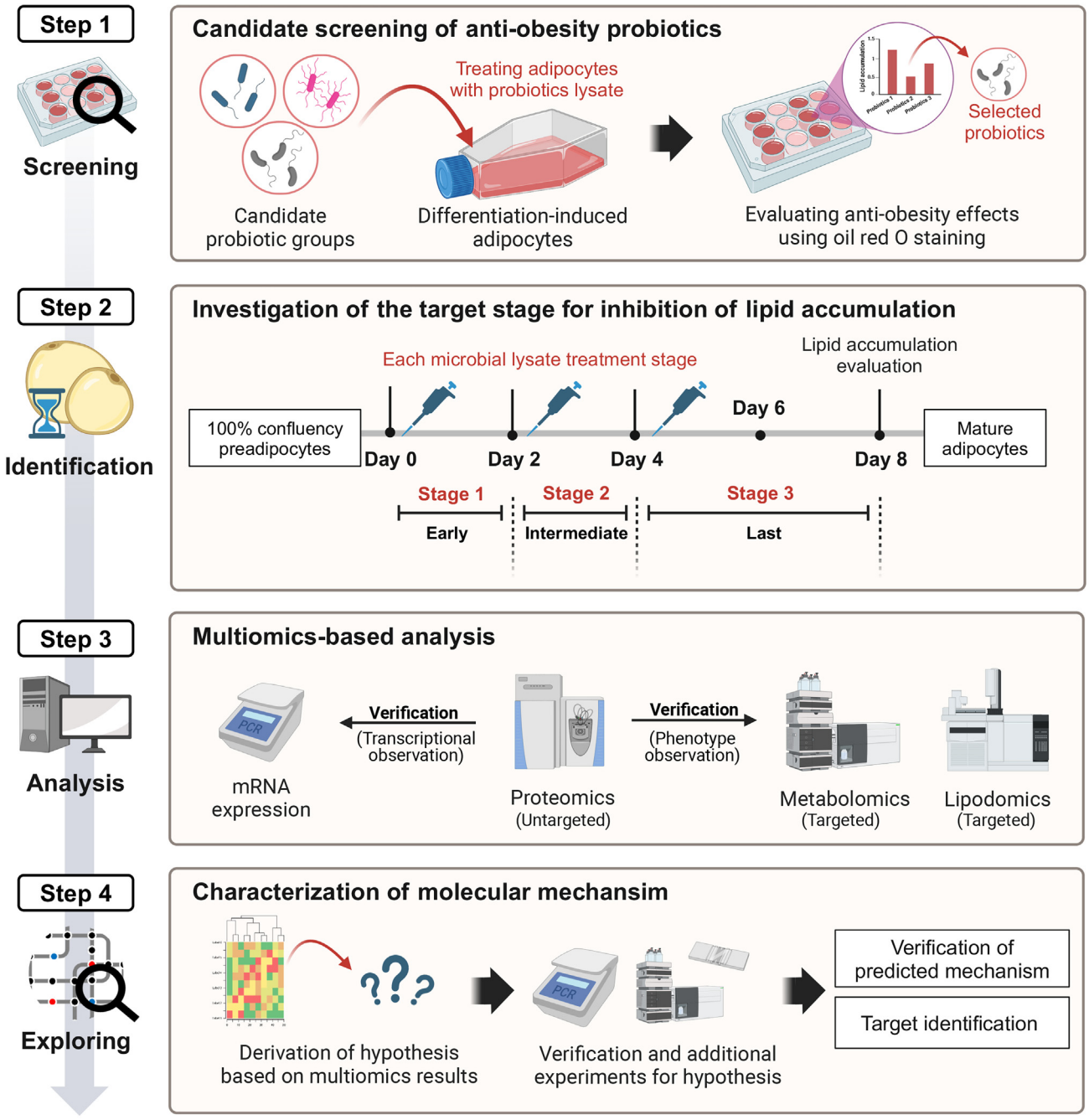

Figure 1. Schematic overview of deciphering the anti-obesity mechanisms of probiotics

An effective probiotic lysate was prepared from the candidate probiotics and applied to adipocytes. The adipocytes were categorized into early, intermediate, and last stages of adipogenesis to identify the stages at which a reduction in lipid accumulation was observed upon treatment. Proteomics analysis was conducted focusing on the identified stages. Analyses of metabolites, lipids, mRNA were performed to validate the proteomic results.

To investigate the impact of *L. reuteri* on major transcription factors involved in the regulation of adipogenesis in adipocytes, we analyzed changes in gene expression of the major factors: peroxisome proliferator-activated receptor γ (PPARγ) and CCAAT/enhancer-binding protein (C/EBPα).[29] At each time point of days 2 and 8 of adipogenesis, mRNA expression of both PPARγ and C/EBPα was decreased compared to the control group (Figure 3D). This result suggested that treatment with *L. reuteri* inhibited the expression of PPARγ and C/EBPα from the early differentiation stage, thus preventing adipocyte differentiation and reducing lipid accumulation. Taken together, our findings revealed the crucial stage at which *L. reuteri* exhibited

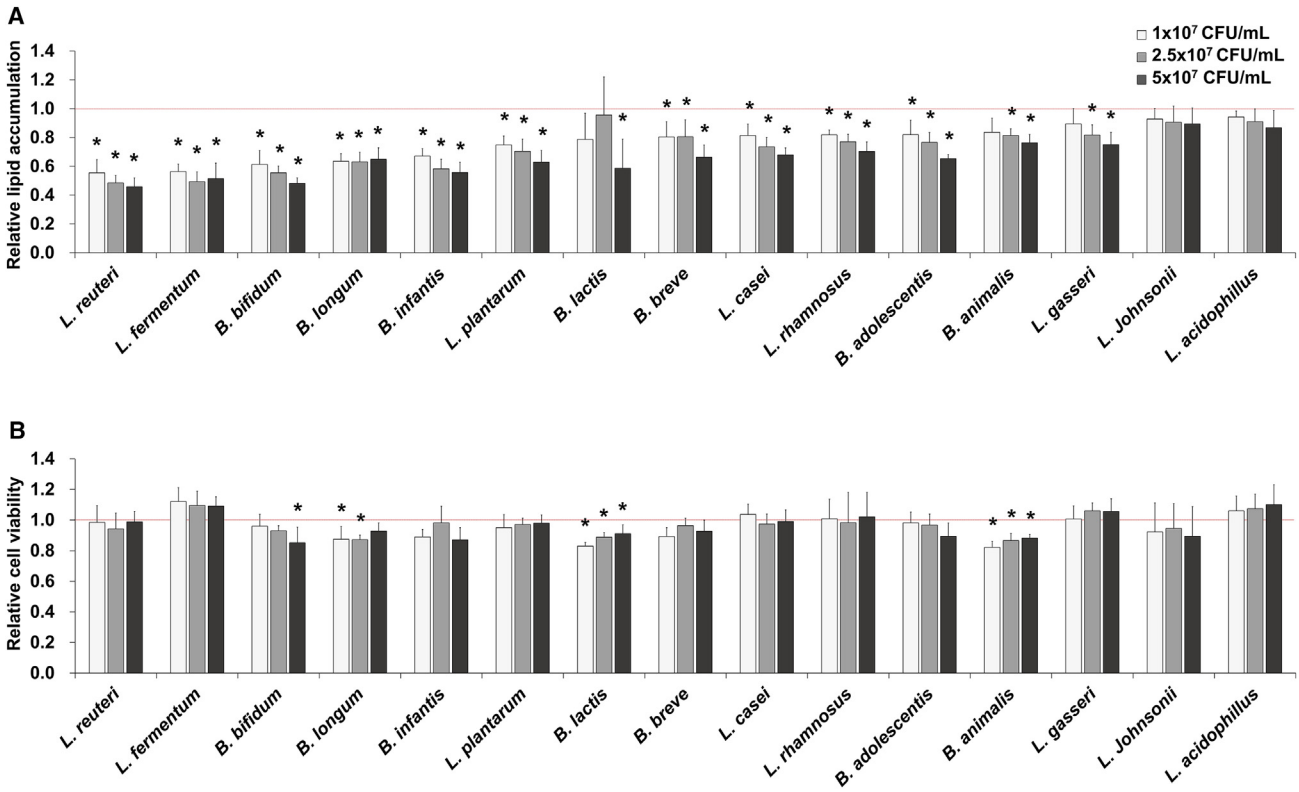

Figure 2. Comparison of the inhibitory effects of probiotic candidates on adipogenesis in 3T3-L1 cells

(A) Comparison of lipid accumulation in 3T3-L1 cells. Lipid accumulation in 3T3-L1 cells treated with probiotic lysates was measured using Oil red O staining ($n = 3$).

(B) Cytotoxicity of probiotic lysates on 3T3-L1 cells. Cell viability was measured by MTT assay ($n = 3$).

Data are represented as means ± SD. Statistical significance was analyzed using one-way ANOVA with Tukey's HSD test and indicated as * for $p < 0.05$ respectively compared with controls.

antiadipogenic potential. This was further confirmed by suppressing PPARγ and C/EBPα expression during early differentiation.

Proteomic changes in adipocytes in early differentiation and maturation stages

To investigate the intracellular proteome changes in adipocytes during treatment with *L. reuteri* lysate from days 0–8, cells were harvested and analyzed at two timepoints—days 2 and 8—after induction of preadipocyte differentiation. Principal component analysis showed a substantial difference in separation between different experimental groups and clustering between biological replicates on both days 2 and 8 (Figure 4A). Additionally, hierarchical clustering analysis of the total proteins detected was used to visualize differences between groups (Figure S3). A total of 3,535 and 2,641 proteins were identified on days 2 and 8, respectively, with 2,340 proteins identified in common between the two datasets (Figure 4B). To analyze differences in protein expression in adipocytes induced by *L. reuteri*, proteins exhibiting a 1.5-fold change and a *p* value of less than 0.05 were classified as differentially expressed proteins (DEPs). On day 2, 128 proteins were classified as DEPs, with 62 upregulated and 66 downregulated proteins. On day 8, 606 proteins were classified as DEPs, with 316 upregulated and 290 downregulated proteins (Figure 4E; Table S1). In addition, 40 proteins were identified as overlapping DEPs at both time points (Figure 4C; Table S2).

Subsequently, to identify the molecular pathways regulated by *L. reuteri* during adipogenesis, Gene Ontology (GO) term and Kyoto Encyclopedia of Genes and Genomes (KEGG) pathway enrichment analysis was performed using ShinyGO 0.80 on the four DEP groups categorized by protein harvest time and differential expression.[30] KEGG pathway enrichment analysis results were shown only for the top 10 with FDR < 0.05 based on fold enrichment (Figure 4F). The downregulated DEPs on day 2 were excluded as no significant enrichment was found. Through GO term and KEGG pathway enrichment analysis, upregulated DEPs in adipocytes treated with *L. reuteri* were mainly involved in iron and glucose metabolism, including the HIF-1 and glucagon signaling pathways, as well as with the composition of cell and organelle membranes. The downregulated DEPs were mainly involved in energy and lipid metabolism, including the tricarboxylic acid (TCA) cycle, BCAA degradation, and fatty acid metabolism, as well as in mitochondrial composition (Figures 4F and S4).

To further focus on the changes in adipogenesis-associated proteins, they were visualized using heatmaps (Figure 4D). The

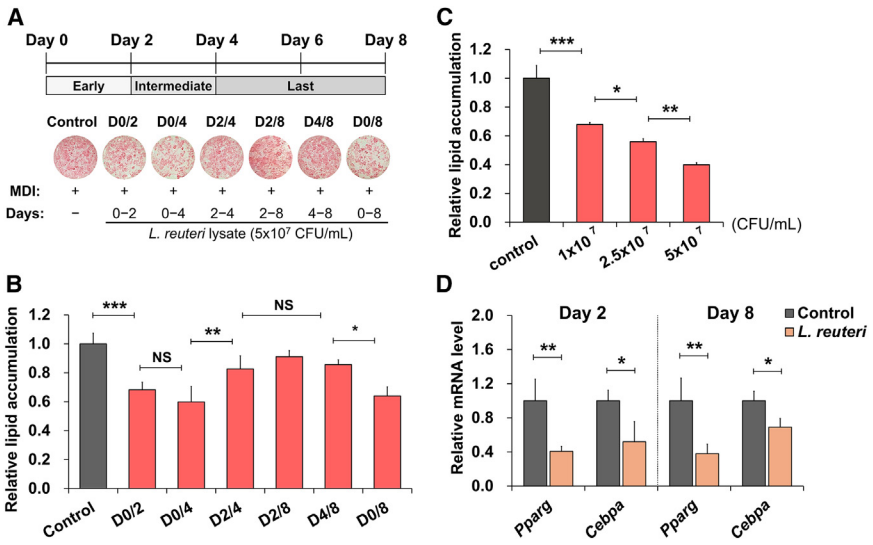

Figure 3. Effect of *L. reuteri* on adipogenesis inhibition

(A) Diagram outlining the stages of the adipogenesis process. *L. reuteri* was treated during different time periods of adipogenesis.

(B) Lipid accumulation was quantified by staining adipocytes with Oil red O staining on day 8 ($n = 6$). Data are represented as means ± SD. Statistical significance was analyzed using one-way ANOVA with Tukey's HSD test and indicated as $^*p < 0.05$, $^{**}p < 0.01$, $^{***}p < 0.001$; ns: no significant.

(C) Lipid accumulation in adipocytes treated with *L. reuteri* under the D0/2 condition ($n = 3$). Data are represented as means ± SD. Statistical significance was analyzed using one-way ANOVA with Tukey's HSD test and indicated as $^*p < 0.05$, $^{**}p < 0.01$, $^{***}p < 0.001$.

(D) Relative mRNA levels of PPARγ and C/EBPα measured in early differentiating (day 2) and mature (day 8) adipocytes, respectively ($n = 4$). Data are represented as means ± SD. Statistical significance was analyzed using unpaired two-tailed Student's t test and indicated as $^*p < 0.05$, $^{**}p < 0.01$, $^{***}p < 0.001$.

downregulated proteins were mainly involved in the PPAR signaling pathway, fatty acid metabolism, and TCA cycle, while the upregulated proteins mainly included proteins involved in the tumor necrosis factor signaling pathway. The changes in most adipogenesis-associated proteins (including SerpinA3g and Fasn) in Figure 4D show a similar pattern to previously reported protein changes in adipocytes in response to other probiotic lysates.[31] This suggested that the MOA of antiadipogenic probiotics on adipocytes may be partially shared.[32]

Inhibition of lipid accumulation through treatment with *L. reuteri* via modulation of BCAA catabolism

To characterize the metabolic changes induced by *L. reuteri*, we investigated enzymatic changes related to energy and lipid metabolisms, which are major metabolic pathways in adipocytes and are shown in Figure 5A. Proteomic analysis was conducted at two time points—early differentiating adipocytes (day 2) and mature adipocytes (day 8)—to investigate changes in energy and lipid metabolisms. Changes in lipid metabolism were confirmed only in mature adipocytes (Figure 5B). Notably, alterations in lipid metabolism were exclusively observed in mature adipocytes. Major energy metabolism processes, including the TCA cycle and oxidative phosphorylation (OXPHOS), occurring in mitochondria exhibited an overall decrease in adipocytes (days 2 and 8) treated with *L. reuteri*, suggesting that it may inhibit mitochondrial function (Figure 5B). The decrease in mitochondrial function was further confirmed by Search Tool for the Retrieval of Interacting Genes/Proteins (STRING)[33] network analysis of downregulated proteins in adipocytes (day 8) (Figure S5). In mature adipocytes, the major source for lipid synthesis is glucose, but BCAAs (isoleucine, leucine, and valine) can also contribute to lipid accumulation.[34] BCAAs participate in the TCA cycle by catabolizing themselves to acetyl-CoA or succinyl-CoA, which is then converted to palmitate (C16:0) and subsequently synthesized into triglycerides through *de novo* lipogenesis to form lipid droplets.[34,35] Our proteomics data showed an overall decrease in enzymes involved in BCAA catabolism (Figure 5B), which could result in their reduced degradation and intracellular accumulation. Generally, BCAA consumption increases gradually during adipocyte differentiation.[35] Because the increase in BCAA catabolism in early adipocyte differentiation promotes adipogenesis prior to PPARγ activation, the level of intracellular BCAAs in adipocytes serves as a crucial indicator for evaluating the inhibition of adipogenesis.[36] Metabolomic analysis was performed in adipocytes to investigate the alteration of BCAA levels according to *L. reuteri* treatment conditions. Interestingly, a significant increase in BCAA levels was observed only in groups (D0/2 and D0/8) treated during early adipocyte differentiation (Figure 5D). In addition, the inhibition of BCAA catabolism in early adipocyte differentiation consequently decreased the production of acetyl-CoA,[34,35] a major precursor in *de novo* lipogenesis, which was observed in adipocytes (D0/2 and D0/8) along with a reduction in malonyl-CoA and palmitoyl-CoA (Figure 5D). At the transcriptional and protein levels, the expression of most genes involved in adipogenesis, including those responsible for transferring acetyl-CoA to palmitoyl-CoA (Fasn, Acaca), fatty acid transporter (Fabp4), and adipocyte marker (Adipoq) expression, was confirmed to be significantly downregulated (Figure 5E). These results confirmed that *L. reuteri* selectively inhibits early adipocyte differentiation, reduces BCAA catabolism, and inhibits adipogenesis before PPARγ activation.

Lipid metabolism in adipocytes is primarily categorized into energy storage, including lipid and fatty acid synthesis, and energy expenditure, including lipolysis and fatty acid oxidation, and is regulated by PPARγ.[37] Inhibition of BCAA catabolism through *L. reuteri* can interfere with adipogenesis, which was confirmed by a decrease in enzymes involved in lipid metabolism (Figure 5C). The decrease in new lipid droplets indicated a decrease in lipid accumulation, which was confirmed by the reduction in Cav1, Plin1, and Cavin1 levels, which are membrane proteins of lipid droplets (Figure 5C). As a component of triglycerides, the end product of lipid metabolism, fatty acids contribute to ATP

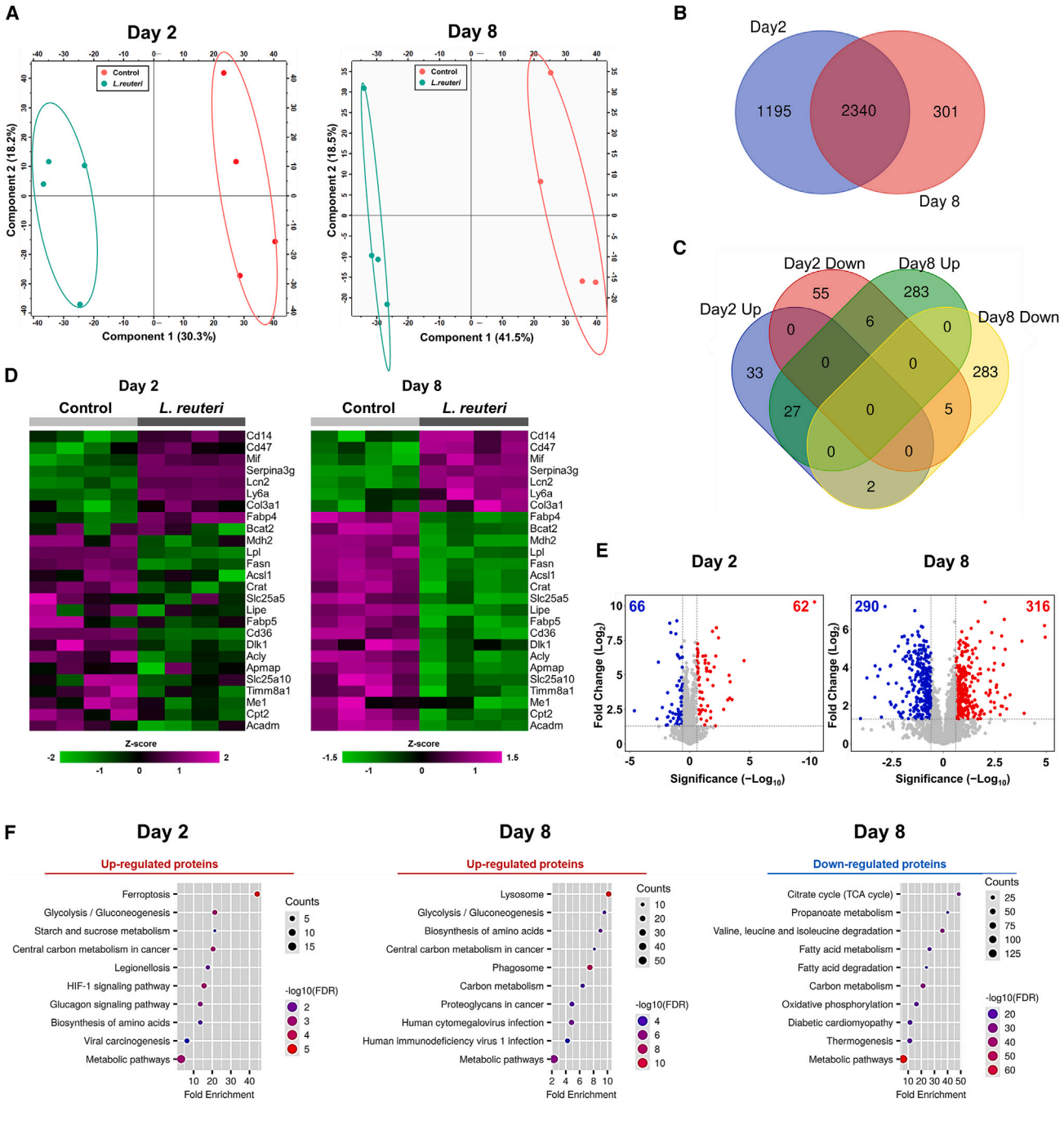

Figure 4. Analysis of intracellular proteome changes in early differentiating (day 2) and mature (day 8) adipocytes in response to *L. reuteri*

(A) Principal component analysis (PCA) from the intracellular proteome of adipocytes treated with *L. reuteri*.

(B and C) Venn diagrams illustrating all identified proteins at each time point and their overlap among differentially expressed proteins.

(D) Heatmap of protein changes associated with adipocyte differentiation, based on a fold change cut-off of >1.5 and $p < 0.05$. The color of heatmap represents the log2 ratio of each protein in each replicate.

(E) Volcano plots showing proteins differentially regulated at each point by *L. reuteri* treatment. Proteins with increased levels compared to the control are shown in red, while decreased proteins are shown in blue. The number of proteins is indicated at each edge of the plot, based on fold change cut-off of >1.5 and $p < 0.05$.

(F) Enrichment analysis performed using ShinyGO for proteins with significant differences, showing the top 10 KEGG pathways based on fold enrichment with an FDR cut-off of <0.05. No significant enrichment was found in proteins that decreased on day 2.

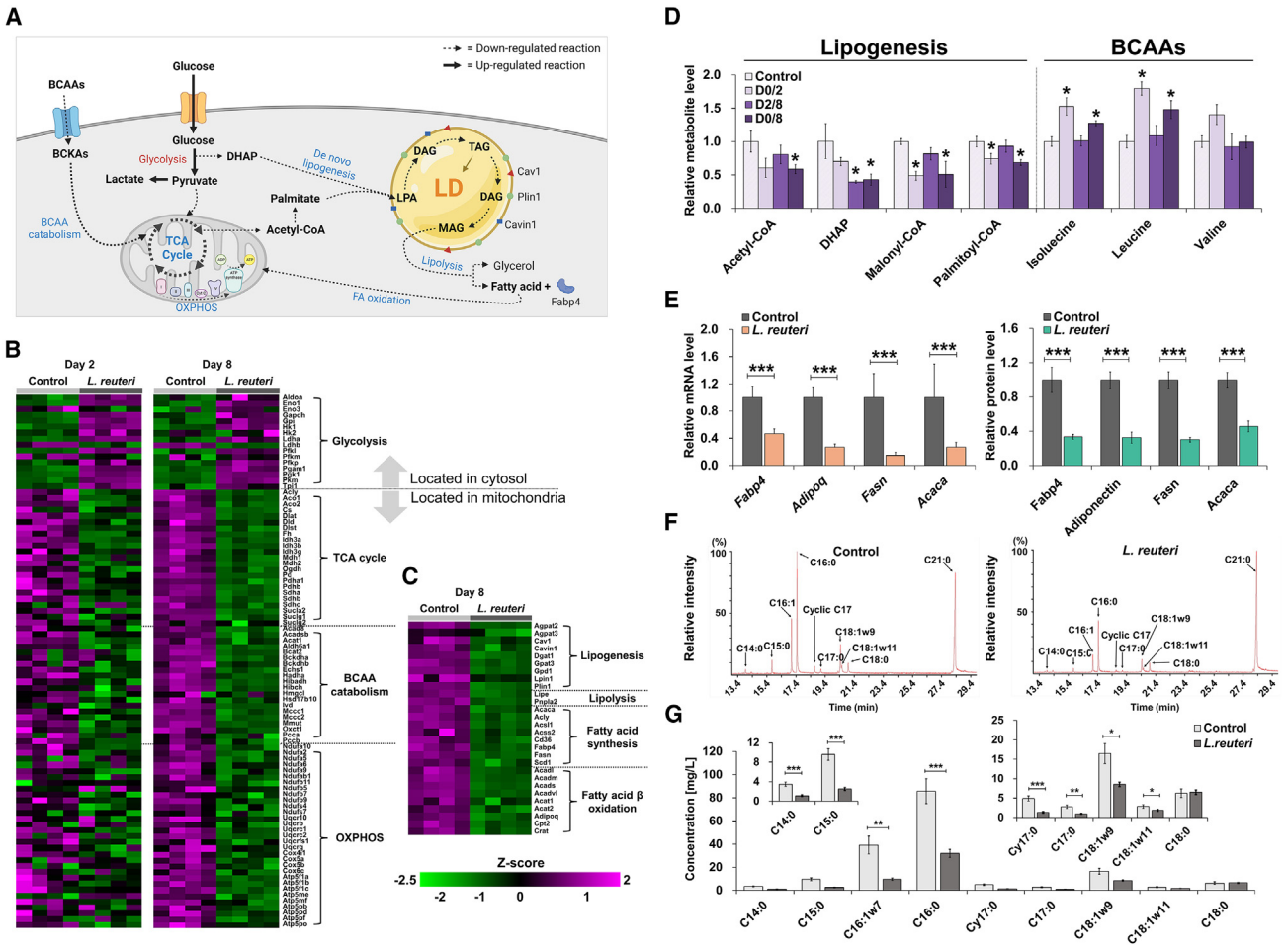

Figure 5. Reducing lipid accumulation by modulating BCAA catabolism with *L. reutri*

(A) Visualization of the major metabolic changes in the adipocytes, including energy metabolism and lipid metabolism.

(B and C) Heatmap of protein changes associated with energy metabolism and lipid metabolism in adipocytes based on fold change cut-off of >1.5 and $p < 0.05$. The color of heatmap represents the log2 ratio of each protein in each replicate ($n = 4$).

(D) Relative levels of lipogenesis-related metabolites and BCAAs during the *L. reuteri* treatment period ($n = 3$).

Data are represented as means ± SD. Statistical significance was analyzed using one-way ANOVA with Tukey's HSD test and indicated as * for $p < 0.05$ respectively compared with controls.

(E) Relative levels of mRNA and protein in mature adipocytes for major factors involved in adipogenesis ($n = 4$).

Data are represented as means ± SD. Statistical significance was analyzed using unpaired two-tailed Student's t test and indicated as *$p < 0.05$, **$p < 0.01$, ***$p < 0.001$.

(F) GC-MS chromatogram of the fatty acid methyl esters (FAMEs) in mature adipocytes using heneicosanoic acid (C21:0) as an internal standard.

(G) Quantification of fatty acids in mature adipocytes with and without *L. reuteri* treatment. The identified fatty acids were quantified using peak area quantification, and the results were subsequently normalized to the internal standard and lipid weight ($n = 3$).

Data are represented as means ± SD. Statistical significance was analyzed using unpaired two-tailed Student's t test and indicated as *$p < 0.05$, **$p < 0.01$, ***$p < 0.001$.

production or promote adipogenesis as signaling molecules.[38,39] Total fatty acid contents were quantified in mature adipocytes by lipidomic analysis to identify changes in fatty acid profiles within adipocytes (Figure 5F). Identified fatty acids all decreased except for stearic acid (C18:0), with fatty acids such as C16:0, C16:1n7 and C18:1n9 collectively constituting approximately 80% of the total fatty acids analyzed in each group (Table S3). Because most fatty acids that constitute lipid droplets are synthesized from acetyl-CoA,[34] its decrease caused by *L. reuteri* can decrease major lipids in adipocytes. Furthermore, odd-chain fatty acids (OCFA; C15:0, and C17:0) are not synthesized from acetyl-CoA but can be synthesized via BCAA catabolism.[40,41] The observed reduction in OCFA is probably due to inhibition of BCAA catabolism.[35,41] Thus, our comprehensive multiomics results, including proteomics, lipidomics, and metabolomics, provide evidence that *L. reuteri* inhibits adipogenesis.

Metabolic alteration induced by *L. reuteri* in adipocytes

Considering that enzymes located in the mitochondria, including most enzymes involved in BCAA catabolism, have decreased

(Figure S5), *L. reuteri* showed the potential to decrease adipogenesis through inhibition of mitochondrial function and subsequently reduce BCAA catabolism. In previous studies, upregulation of mitochondrial metabolism in adipocytes has been reported to promote adipogenesis by producing metabolic intermediates important for essential metabolic processes such as *de novo* lipogenesis rather than simply being a consequence of adipogenesis.[34,42] Furthermore, the maintenance of these metabolic processes depends on a continuous ATP supply.[43] Therefore, inhibition of mitochondrial function by *L. reuteri* may decrease adipogenesis by disrupting the supply of metabolic intermediates and ATP. Interestingly, although mitochondrial function was reduced in adipocytes treated with *L. reuteri*, intracellular ATP levels did not show any significant changes (Figure 6A). Based on this, it was hypothesized that ATP levels were maintained by an alternative pathway that operated in the cytosol rather than the mitochondria. Under normal circumstances, adipocytes commonly generate ATP through OXPHOS in the mitochondria, but under conditions of inhibited mitochondrial function, glycolysis operates as an alternative pathway for ATP production.[44] In our analysis of protein profiles, we observed an increase in glycolytic enzymes following treatment with *L. reuteri*. Based on these findings, we consider glycolysis an alternative pathway for ATP production (Figure 5B). Pyruvate, derived from glucose, can undergo mitochondrial metabolism or be converted to lactate, the end product.[45] Accumulation of lactate, observed in conditions of reduced mitochondrial function, indicates activation of glycolysis.[45,46] Lactate accumulation is regulated by two isoforms of lactate dehydrogenase (LDH). Notably, in our proteomic analysis results, LDHA, which converts pyruvate to lactate, increased. Conversely, LDHB, which converts lactate to pyruvate, decreased (Figure 5B). This modulation of glycolytic activity may result in decreased glucose levels and increased lactate levels, consistent with changes observed in metabolomic analysis performed in early differentiating adipocytes (Figure 6A). As a result, *L. reuteri* inhibited mitochondrial function and induced glycolysis, activating an alternative pathway for ATP production. The increase in glycolysis resulting from reduced mitochondrial function, induced by *L. reuteri*, indicated the inhibition of adipogenesis through reduced BCAA catabolism.[47]

Our multiomics results confirmed that *L. reuteri* effectively reduced mitochondrial function, attenuating adipogenesis. However, this raised the question of whether these actions induced short-term modifications or irreversible impairment of mitochondrial metabolism in early differentiating adipocytes. Therefore, it was necessary to investigate the duration and reversibility of changes induced by *L. reuteri*. To determine whether glycolysis was altered in mature adipocytes depending on *L. reuteri* treatment, additional metabolic analyses were conducted, considering whether the lysate was administered on day 2 before or after differentiation induction (Figures 6B and S6). Interestingly, contradictory results were observed in the D0/2 and D0/8 groups in terms of changes in intracellular lactate levels at day 8, despite both groups experiencing adipogenesis inhibition due to *L. reuteri* treatment during the early differentiation period (Figure 6D). First, D0/8 exhibited an increasing trend in lactate levels that was sustained by *L. reuteri* treatment until day 8, even after initial differentiation. By contrast, after day 2, the lactate levels decreased significantly in D0/2, where the *L. reuteri* treatment was not performed. Additionally, lactate levels increased in D2/8 treated with *L. reuteri* from day 2 onward, indicating that lactate production was induced by *L. reuteri* treatment in the D0/8 and D2/8 groups. Given the earlier observation of increased lactate levels in adipocytes undergoing early differentiation following treatment with *L. reuteri*, it seems probable that exposure to the lysate at the time of cell acquisition is the determining factor of this alteration, suggesting that the observed metabolic changes are a transient effect that occurs specifically during exposure to *L. reuteri*. To provide further evidence for this transient metabolic alteration, we performed an additional search for metabolites associated with glycolysis that showed similar changes in D0/8 and D2/8 (Figure 6C).

It is possible that the metabolic alteration caused by *L. reuteri* was due to decreased mitochondrial function, similar to the observation on day 2. When mitochondrial function is inhibited, nitric oxide (NO) production can be stimulated to restore it in cells with activated glycolysis.[48] NO is generated from arginine through a process that involves its conversion to citrulline.[48] To test our hypothesis that *L. reuteri* inhibits mitochondrial function only during transient exposure, we assessed changes in arginine and its precursor citrulline—essential components of NO production. We observed significant differences only in adipocytes at early differentiating and in groups D2/8 and D0/8, which were exposed to *L. reuteri* at the time of cell acquisition (Figures 6E and 6F). The notable decrease in arginine and the corresponding increase in citrulline in the adipocyte groups exposed to *L. reuteri* indirectly prove that the mitochondrial function of adipocytes was transiently inhibited. In addition, the decreased production of dihydroxyacetone phosphate (DHAP), a precursor of lipid components produced from glucose, at D2/8 and D0/8, suggests the enhancement of the glycolytic pathway leading to lactate production, supporting the possibility of transient metabolic changes induced by *L. reuteri* (Figure 6G). These metabolic changes induced by *L. reuteri* can be restored to their previous state by controlling the treatment process. This implies that *L. reuteri* did not induce mitochondrial damage and did not negatively affect cell survival. In contrast, the inhibition of adipogenesis by *L. reuteri* at the early differentiation stage of adipocytes was irreversible, even when the experimental conditions were controlled. These observations suggest that the effect of *L. reuteri* on early differentiating adipocytes is important in regulating overall adipocyte differentiation. In conclusion, our findings underscore the importance of the timing of early adipocyte differentiation for *L. reuteri* to exert specific and temporally controlled inhibition of adipogenesis.

Inhibition of adipogenesis by interference with KLF5 transcription during early adipocyte differentiation

Major transcription factors and enzymes were investigated to identify potential targets of *L. reuteri*, focusing on C/EBPβ and C/EBPδ, which are crucial regulators expressed during early adipocyte differentiation.[49] In addition, enzymes involved in mitotic clonal expansion (MCE), a process that occurs during early adipocyte differentiation, were also considered potential targets.[50] C/EBPβ and C/EBPδ are expressed early in

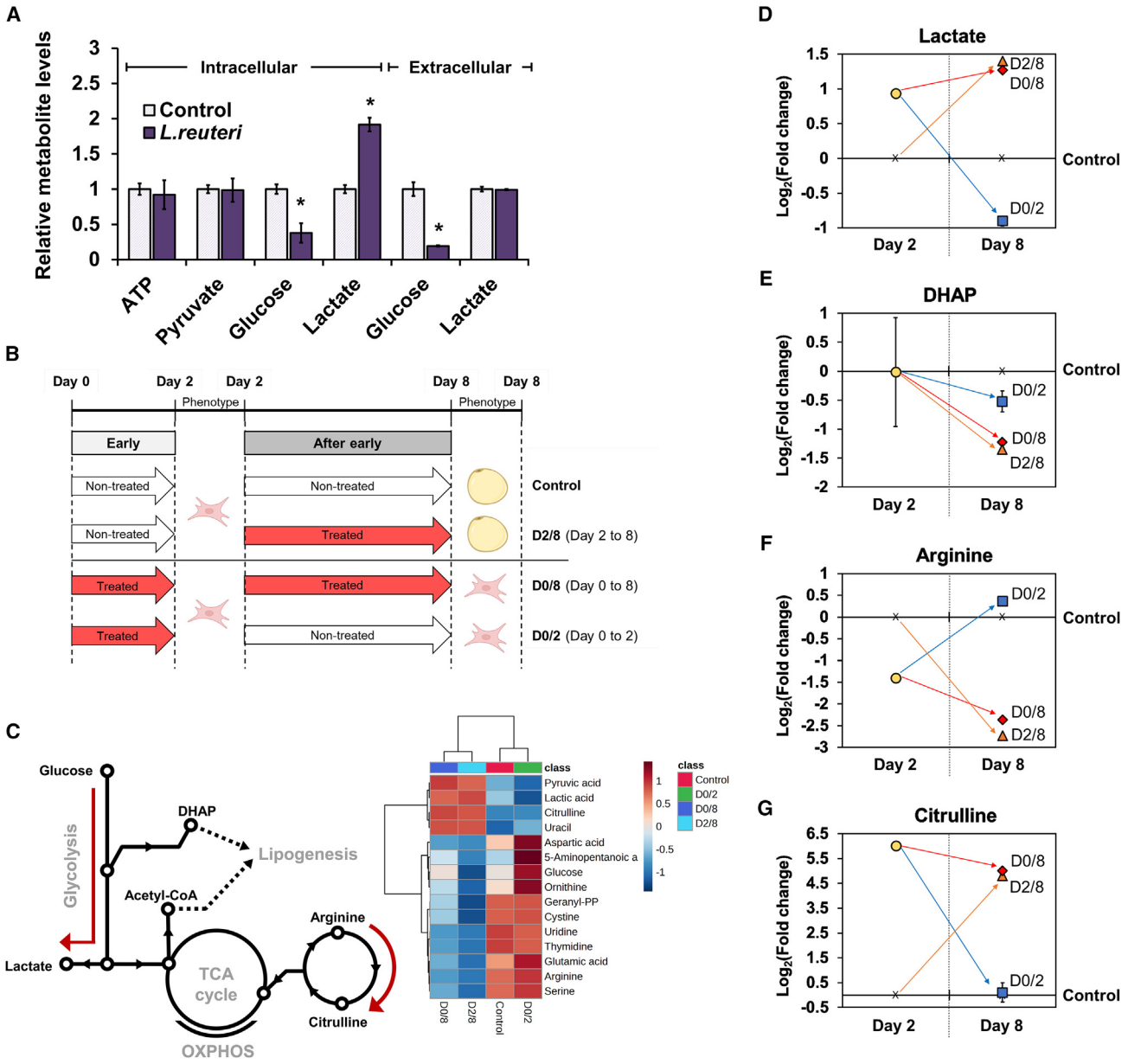

Figure 6. Effect of *L. reuteri* on mitochondrial metabolism in adipocytes

(A) Relative levels of intracellular or extracellular metabolites involved in energy metabolism in early differentiating adipocytes.

Data are represented as means ± SD. Statistical significance was analyzed using unpaired two-tailed Student's t test and indicated as $^{*}p < 0.05$, $^{**}p < 0.01$, $^{***}p < 0.001$.

(B) Schematic for the processing of *L. reuteri* treatment during adipogenesis. Previous results on the differentiation of adipocytes, depending on the timing of *L. reuteri* treatment, were also shown.

(C) Illustration of metabolic pathways activated during exposure to *L. reuteri*, accompanied by a heatmap of the involved metabolites.

(D–G) Changes in lactate (D), citrulline (E), arginine (F), and DHAP (G) between early differentiating (day 2) and mature (day 8) adipocytes in response to the time-point analysis of *L. reuteri* treatment.

adipogenesis initiated by adipogenic cocktails and directly induce expression of PPARγ and CEBPα.[49] In our results, we identified decreased PPARγ and CEBPα expression in early differentiating adipocytes (Figure 3D). This suggests that there is a possibility of inhibition at the pre-expression and postexpression stages of C/EBPβ and C/EBPδ before PPARγ and CEBPα expression. An adipogenic cocktail containing 3-isobutyl-1-methylxanthine (IBMX), dexamethasone (DEX), and insulin induce the expression of C/EBPβ and C/EBPδ through the activation of cAMP response element-binding protein (CREB), glucocorticoid receptor, and sterol regulatory element-binding protein 1 (Srebp1), respectively.[51] In order to

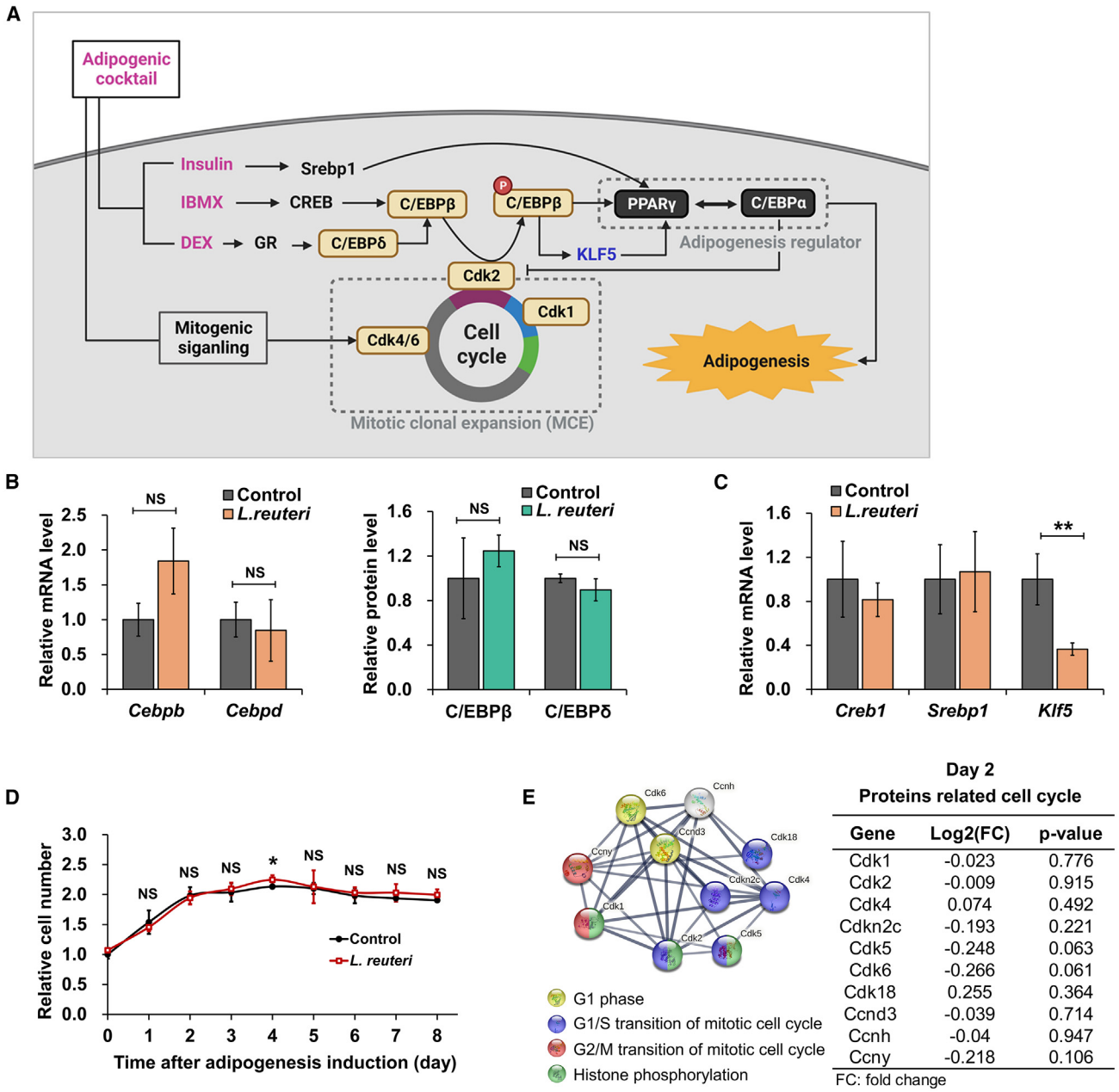

Day 2
Proteins related cell cycle

Gene	Log2(FC)	p-value
Cdk1	-0.023	0.776
Cdk2	-0.009	0.915
Cdk4	0.074	0.492
Cdkn2c	-0.193	0.221
Cdk5	-0.248	0.063
Cdk6	-0.266	0.061
Cdk18	0.255	0.364
Ccnd3	-0.039	0.714
Ccnh	-0.04	0.947
Ccny	-0.218	0.106

FC: fold change

Figure 7. Investigation of transcription factors that regulate early adipocyte differentiation and associated processes

(A) Visualization of overall transcription factor expression and processes occurring during early adipocyte differentiation.

(B) Relative mRNA expression and protein levels of C/EBPβ and C/EBPδ, key regulators in early adipocyte differentiation, in early differentiating adipocyte ($n = 4$).

(C) Relative mRNA expression levels of major factors involved in PPARγ expression in early differentiating adipocytes ($n = 4$).

(D) Effects of *L. reuteri* on the proliferation of adipocytes during early differentiation ($n = 4$). 3T3-L1 preadipocytes at day 0 served as a control.

(E) The protein-protein interaction (PPI) network and a table of changes in proteins involved in the cell cycle are presented.

Data are represented as means ± SD. Statistical significance was analyzed using unpaired two-tailed Student's t test and indicated as $^{*}p < 0.05$, $^{**}p < 0.01$, $^{***}p < 0.001$; ns: no significant.

specify the location of the target before and after C/EBPβ/δ expression, changes were confirmed by examining the mRNA and protein levels of C/EBPβ and C/EBPδ (Figure 7B). However, the analysis found no significant changes in either transcription factor. Consequently, it can be concluded that potential targets of *L. reuteri* remained after C/EBPβ/δ expression. The absence of significant changes in the mRNA expression of Creb1 and Srebp1, transcription factors that regulate C/EBPβ and C/EBPδ expression, indirectly suggested that adipogenesis may be inhibited following C/EBPβ/δ expression (Figure 7C).

C/EBPβ is activated through a phosphorylation process to upregulate PPARγ to promote adipogenesis, and the cell cycle is partially involved in this process. Confluent preadipocytes reenter the cell cycle and undergo MCE, which increases the activity of Cdk2. Activated Cdk2 participates in the phosphorylation of C/EBPβ, promoting its expression as PPARγ.[50,52] To evaluate the changes in C/EBPβ activity, we investigated the impact of *L. reuteri* on MCE by measuring cell counts during adipogenesis. Cell counts showed normal proliferation, with no significant difference observed compared to the control group, and proliferation was nearly complete by day 2 (Figure 7D). Additionally, changes in cell cycle-related enzymes were not significant, suggesting that *L. reuteri* does not affect C/EBPβ activity via MCE (Figure 7E). Therefore, the expression and activation of C/EBPβ remained largely unchanged, and it became apparent that the reduction in PPARγ expression occurred independently of C/EBPβ. Considering the preceding result, we hypothesized that *L. reuteri* might regulate PPARγ expression through modulation of transcription factors downstream of C/EBPβ, including Krüppel-like factor 5 (KLF5), which is considered a strong potential candidate. During early adipocyte differentiation, C/EBPβ binds to the promoter of KLF5 and induces its expression.[53] Moreover, C/EBPβ cooperates with induced KLF5 to bind directly to the promoter of PPARγ, thereby promoting its expression.[53] Indeed, mRNA expression analysis was conducted to confirm the hypothesis that KLF5 could be a target of *L. reuteri*. It was found that the expression of KLF5 decreased in early differentiating adipocytes (Figure 7C). Consequently, *L. reuteri* reduced PPARγ expression by downregulating KLF5 transcription. Additionally, the reduction of KLF5 resulted in the downregulation of transcription factors induced by it. In adipocytes, KLF5 promotes BCAA catabolism by inducing the expression of Krüppel-like factor 15 (KLF15).[54,55] This suggests that a reduction in KLF5 may attenuate BCAA catabolism, consistent with previously observed changes in BCAA metabolism (Figure 5A). In conclusion, KLF5 is a crucial target of *L. reuteri* in reducing adipogenesis by interfering with early adipocyte differentiation, and the observed changes in adipocyte metabolism strongly support this conclusion.

Investigating HIF-1α as a target for *L. reuteri* in inhibiting adipogenesis

Based on previous research results, it was validated that *L. reuteri* exhibited specific and temporal effects in inhibiting adipogenesis (Figure 6). Considering the metabolic changes induced by *L. reuteri* as transient responses, we hypothesized that the factors regulating these metabolic changes could be additional targets. To identify these additional targets, we explored the enrichment analysis results presented in Figure 4F, focusing on pathways that could induce metabolic changes. Treatment with L. *reuteri* increased iron and glucose metabolism in adipocytes on days 2 and 8. Furthermore, an increase in HIF-1 signaling, which may regulate these metabolic changes, was identified specifically in adipocytes on day 2. This suggests that the activation of HIF-1 signaling potentially influences metabolic changes in adipocytes. In general, HIF-1α, a crucial transcription factor of HIF-1 signaling and a metabolic regulator induced by hypoxia,[56] increased in early differentiating adipocytes through mRNA expression analysis (Figure 8A). Activation of HIF-1 signaling stimulates glycolysis by upregulating phosphoglycerate kinase 1 (PGK1) and lactate dehydrogenase A (LDHA) while concurrently inhibiting pyruvate dehydrogenase (PDH) through increased expression of pyruvate dehydrogenase kinase 1 (PDK1), which suppresses the entry of pyruvate into the TCA cycle.[57] This metabolic modulation aligns with the observed changes in adipocytes treated with *L. reuteri* and provides evidence supporting the activation of HIF-1 signaling (Figure 5B). Moreover, the increase in HIF-1α levels in adipocytes can result in reduced BCAA catabolism, consistent with prior research findings.[58,59] HIF-1 signaling might have been activated through hypoxia induced by *L. reuteri*, but not all metabolic processes regulated under hypoxia are dependent on HIF-1α.[57] This implies that by investigating alternative pathways, it is possible to determine whether the increase in HIF-1α is independent of or dependent on hypoxia. Recent studies have demonstrated that hypoxia can activate the Nuclear Factor κ-light-chain-enhancer of activated B cells (NF-κB) pathway in adipocytes, particularly the canonical NF-κB pathway regulated by IκB kinase (IKK).[60] In our results, most enzymes involved in the canonical NF-κB pathway did not show significant changes (Figure 8B). According to the results, HIF-1 signaling is activated independently of hypoxia, suggesting that this may be a response to specific substances within *L. reuteri* rather than environmental changes resulting from *L. reuteri* treatment. Given that most metabolic changes in adipocytes treated with *L. reuteri* involve HIF-1 signaling, HIF-1α can be considered another potential target of *L. reuteri* contributing to the suppression of adipogenesis.

For HIF-1α to be recognized as a target to inhibit adipogenesis, it must selectively act in early adipocyte differentiation and interfere with adipogenesis. Previous studies investigating the impact of HIF-1α on adipogenesis have reported its dual effect, involving lipid accumulation and inhibition.[61] The reported adipogenic effect of HIF-1α is predominantly association with mature adipocytes,[61] whereas the antiadipogenic effect is predominantly association with differentiating adipocytes.[61] These reports suggest that the role of HIF-1α differ depending on the adipocyte differentiation stage. The effect of HIF-1α is consistent with the effect of *L. reuteri* in selectively targeting early adipocyte differentiation, which consequently means that HIF-1α can be considered a target of *L. reuteri*. To explore the mechanism through which elevated levels of HIF-1α may influence early adipocyte differentiation, we investigated the transcription factors that potentially affect lipid metabolism and are activated by HIF-1α. We focused on the fact that the expression of lipin-1 in adipocytes can be induced by HIF-1α.[62] Interestingly, HIF-1α reduces the expression of lipin-1 in differentiating adipocytes and increases its expression in mature adipocytes.[63] Lipin-1 has two isoforms, lipin-1α, which is expressed during early differentiation of adipocytes and promotes adipogenesis, and lipin-1β, which is expressed in adipocytes and involved in lipid accumulation, and its expression is regulated by RNA splicing.[64] This suggests that HIF-1α upregulates the expression of lipin-1β while downregulating the expression of lipin-1α, suggesting a possible differential effect as a result of the regulation of lipin-1 depending on the timing of adipocyte differentiation. Based on previous studies, we hypothesized that *L. reuteri* could

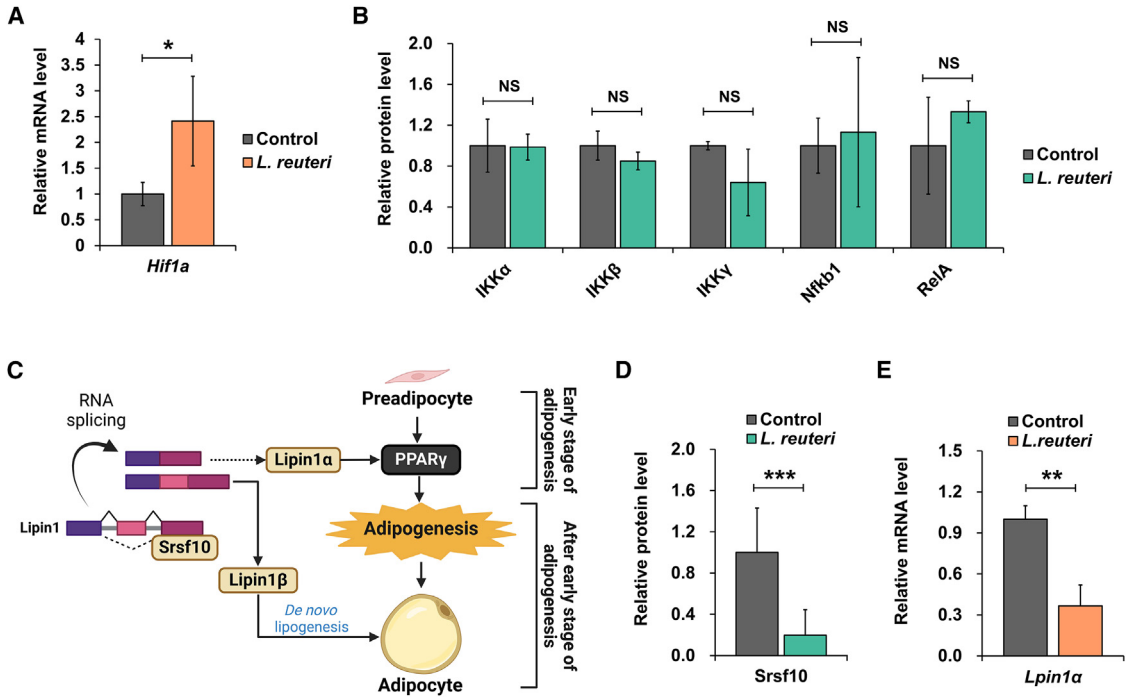

Figure 8. HIF-1α as a potential target for *L. reuteri* in adipogenesis inhibition

(A) Relative mRNA expression of HIF-1α and (n = 4).

(B) Relative mRNA expression levels of major factors involved in the canonical NF-κB pathway in early differentiating adipocytes (n = 4).

(C) Illustration of lipin-1 isoform expression by RNA splicing.

(D) Relative protein levels in early differentiating adipocytes (n = 4).

(E) Relative mRNA level of lipin-1α in early differentiating adipocytes (n = 4).

Data are represented as means ± SD. Statistical significance was analyzed using unpaired two-tailed Student's t test and indicated as *p < 0.05, **p < 0.01, ***p < 0.001; ns: no significant.

inhibit early adipogenesis by reducing the expression of lipin-1α. Thus, we investigated the changes in serine/arginine splicing factor 10 (Srsf10), an enzyme involved in the RNA splicing of lipin-1. In our results, Srsf10 was found to be significantly reduced in early differentiating adipocytes (Figure 8D). This decrease in Srsf10 may eventually lead to a reduction in lipin-1α expression, which was confirmed through additional mRNA expression analysis (Figure 8E). Therefore, it was suggested that *L. reuteri* can inhibit early adipocyte differentiation by reducing lipin-1 through upregulation of HIF-1α and subsequent reduction of Srsf10. Furthermore, HIF-1α induces metabolic changes in adipocytes in response to *L. reuteri*, inhibiting adipogenesis during early differentiation.

Conclusions

Our advanced multiomics strategy identifies the critical treatment period in which *L. reuteri* effectively exhibits the anti-obesity effect and identifies the molecular mechanism inhibiting adipogenesis through multiomics analysis. In exploring the intricate mechanisms underlying adipogenesis, this study delves into the specific inhibition of BCAA catabolism by *L. reuteri* during early differentiation—a critical juncture that may pivot toward lipid production. Our findings illuminate how *L. reuteri* orchestrates a nuanced modulation of adipocyte differentiation by simultaneously decreasing KLF5 and increasing HIF-1α, initiating a cascade that leads to the attenuation of BCAA catabolism and PPARγ expression, resulting in the suppression of adipogenesis. This dual modulation not only highlights KLF5 and HIF-1α as pivotal targets of the action of *L. reuteri* but also unravels the connection between KLF5 and BCAA catabolism. Such insights extend our understanding regarding the regulatory pathways in adipogenesis, suggesting new angles of investigation. Moreover, the efficacy of our advanced multiomics strategy in uncovering these novel mechanisms and target molecules emphasizes potential of this approach in identifying the probiotic-regulated pathways of adipogenesis inhibition. Therefore, our advanced multiomics strategy has successfully elucidated the complex causal dynamics of adipocytes and microorganisms and identified critical targets for probiotics to exhibit anti-obesity properties. Probiotics demonstrating beneficial effects on obesity are promising candidates for the next generation of obesity treatment. Systematically identifying the MOA and targets through validated methods is crucial for their development as treatments.

Limitations of the study

In this study, we proposed a multiomics-based strategy to elucidate the suppression mechanism of potential probiotics on lipid formation. By providing complementary validation through integrated multiomics data, we gained insights into the putative

mechanisms by which probiotics inhibit lipid formation and identified potential target proteins. However, to confirm whether these proposed mechanisms function as hypothesized, additional validation through experiments using knock-out or overexpression models targeting these proteins is necessary. Nevertheless, given the importance of a molecular understanding of the complex mechanisms of adipocytes in characterizing anti-obesity effects, this multiomics-based in-depth/systematic approach could serve as a foundational framework for future research. Additionally, to evaluate the anti-obesity effects of live probiotics more robustly, it is crucial to consider extending this strategy to host-microbe interaction coculture platforms and *in vivo* models.

RESOURCE AVAILABILITY

Lead contact

Further information and requests for resources and reagents should be directed to and will be fulfilled by the lead contact, Yun-Gon Kim (ygkim@ssu.ac.kr).

Materials availability

This study did not generate new unique reagents.

Data and code availability

- The mass spectrometry proteomics data have been deposited at ProteomeXchange Consortium via the PRIDE partner repository. The mass spectrometry metabolomics data have been deposited at the MetaboLights database. Both datasets are listed in the key resources table and publicly available as of the date of publication. (PRIDE: PXD050884 and Metabolight: MTBLS12185).
- This paper does not report any original code.
- Any additional information required to reanalyze the data reported in this paper is available from the lead contact upon request.

ACKNOWLEDGMENTS

This work was supported by the Basic Science Research Program through the National Research Foundation of Korea (NRF) grant funded by the Korean government (NRF-2017M3A9E4077235, NRF-2020R1A6A1A03044977, and NRF-2022R1F1A1073595). This work was also supported by CJ CheilJedang Corporation.

AUTHOR CONTRIBUTIONS

Y.-R.K. and Y.-G.K. designed the experiments. Y.-G.K. obtained the funding for the study. Y.-R.K. conducted experiments and analyzed the data. M.-G.K., J.-H.B., S.-Y.K., and B.-G.C. assisted in screening anti-obesity probiotics. S.-H.J. assisted in proteomics measurements. T.-R.C. and Y.-H.Y. performed lipidomics measurements. Y.-R.K. and Y.-G.K. wrote and revised the draft of manuscript. W.-S.S., C.-S.J., T.H.K., S.-H.J., and S.W.S. reviewed the final version of the manuscript. All authors have read and approved the submitted manuscript.

DECLARATION OF INTERESTS

The authors declare no competing interests.

STAR★METHODS

Detailed methods are provided in the online version of this paper and include the following:

SUPPLEMENTAL INFORMATION

Supplemental information can be found online at https://doi.org/10.1016/j.isci.2025.111890.

Received: June 4, 2024
Revised: October 23, 2024
Accepted: January 22, 2025
Published: January 25, 2025

REFERENCES

1. Chooi, Y.C., Ding, C., and Magkos, F. (2019). The epidemiology of obesity. Metabolism *92*, 6–10.
2. World Health Organization (2000). Obesity: Preventing and Managing the Global Epidemic: Report of a WHO Consultation, World Health Organization - Technical Report Series, 894.
3. Kopelman, P.G. (2000). Obesity as a medical problem. Nature *404*, 635–643.
4. Rössner, S. (2002). Obesity: the disease of the twenty-first century. Int. J. Obes. *26*, S2–S4.
5. Hariri, N., and Thibault, L. (2010). High-fat diet-induced obesity in animal models. Nutr. Res. Rev. *23*, 270–299.
6. McAllister, E.J., Dhurandhar, N.V., Keith, S.W., Aronne, L.J., Barger, J., Baskin, M., Benca, R.M., Biggio, J., Boggiano, M.M., Eisenmann, J.C., et al. (2009). Ten putative contributors to the obesity epidemic. Crit. Rev. Food Sci. Nutr. *49*, 868–913.
7. Bray, G.A., Frühbeck, G., Ryan, D.H., and Wilding, J.P.H. (2016). Management of obesity. Lancet *387*, 1947–1956.
8. Müller, T.D., Blüher, M., Tschöp, M.H., and DiMarchi, R.D. (2022). Anti-obesity drug discovery: advances and challenges. Nat. Rev. Drug Discov. *21*, 201–223.
9. Fuller, R. (1989). Probiotics in man and animals. J. Appl. Bacteriol. *66*, 365–378.
10. Salminen, S., Collado, M.C., Endo, A., Hill, C., Lebeer, S., Quigley, E.M.M., Sanders, M.E., Shamir, R., Swann, J.R., Szajewska, H., and Vinderola, G. (2021). The International Scientific Association of Probiotics and Prebiotics (ISAPP) consensus statement on the definition and scope of postbiotics. Nat. Rev. Gastroenterol. Hepatol. *18*, 649–667.
11. Aguilar-Toalá, J., Garcia-Varela, R., Garcia, H., Mata-Haro, V., González-Córdova, A., Vallejo-Cordoba, B., and Hernández-Mendoza, A. (2018). Postbiotics: An evolving term within the functional foods field. Trends Food Sci. Technol. *75*, 105–114.
12. Turnbaugh, P.J., Ley, R.E., Mahowald, M.A., Magrini, V., Mardis, E.R., and Gordon, J.I. (2006). An obesity-associated gut microbiome with increased capacity for energy harvest. Nature *444*, 1027–1031.
13. Cani, P.D., and Delzenne, N.M. (2011). The gut microbiome as therapeutic target. Pharmacol. Ther. *130*, 202–212.
14. Snigdha, S., Ha, K., Tsai, P., Dinan, T.G., Bartos, J.D., and Shahid, M. (2022). Probiotics: Potential novel therapeutics for microbiota-gut-brain

axis dysfunction across gender and lifespan. Pharmacol. Ther. *231*, 107978.

15. Marco, M.L., Pavan, S., and Kleerebezem, M. (2006). Towards understanding molecular modes of probiotic action. Curr. Opin. Biotechnol. *17*, 204–210.
16. Kong, C., Gao, R., Yan, X., Huang, L., and Qin, H. (2019). Probiotics improve gut microbiota dysbiosis in obese mice fed a high-fat or high-sucrose diet. Nutrition *60*, 175–184.
17. Borgeraas, H., Johnson, L.K., Skattebu, J., Hertel, J.K., and Hjelmesaeth, J. (2018). Effects of probiotics on body weight, body mass index, fat mass and fat percentage in subjects with overweight or obesity: a systematic review and meta-analysis of randomized controlled trials. Obes. Rev. *19*, 219–232.
18. Parkkinen, V.-P., Wallmann, C., Wilde, M., Clarke, B., Illari, P., Kelly, M.P., Norell, C., Russo, F., Shaw, B., and Williamson, J. (2018). Evaluating Evidence of Mechanisms in Medicine: Principles and Procedures (Springer Nature).
19. Turroni, F., Ventura, M., Buttó, L.F., Duranti, S., O'Toole, P.W., Motherway, M.O., and van Sinderen, D. (2014). Molecular dialogue between the human gut microbiota and the host: a Lactobacillus and Bifidobacterium perspective. Cell. Mol. Life Sci. *71*, 183–203.
20. Zhang, A., Sun, H., and Wang, X. (2013). Power of metabolomics in biomarker discovery and mining mechanisms of obesity. Obes. Rev. *14*, 344–349.
21. Papadimitriou, K., Zoumpopoulou, G., Foligné, B., Alexandraki, V., Kazou, M., Pot, B., and Tsakalidou, E. (2015). Discovering probiotic microorganisms: *in vitro*, *in vivo*, genetic and omics approaches. Front. Microbiol. *6*, 58.
22. Jo, S.-H., Jeon, H.-J., Song, W.S., Lee, J.S., Kwon, J.E., Park, J.H., Kim, Y.R., Kim, M.G., Baek, J.H., Kwon, S.Y., et al. (2023). Unveiling the inhibition mechanism of Clostridioides difficile by Bifidobacterium longum via multiomics approach. Front. Microbiol. *14*, 1293149.
23. Guru, A., Issac, P.K., Velayutham, M., Saraswathi, N.T., Arshad, A., and Arockiaraj, J. (2021). Molecular mechanism of down-regulating adipogenic transcription factors in 3T3-L1 adipocyte cells by bioactive anti-adipogenic compounds. Mol. Biol. Rep. *48*, 743–761.
24. Herold, C., Rennekampff, H.O., and Engeli, S. (2013). Apoptotic pathways in adipose tissue. Apoptosis *18*, 911–916.
25. Fåk, F., and Bäckhed, F. (2012). Lactobacillus Reuteri Prevents Diet-Induced Obesity, but Not Atherosclerosis, in a Strain Dependent Fashion in Apoe−/− Mice (Public Library of Science San Francisco).
26. Hsieh, F.-C., Lan, C.-C.E., Huang, T.-Y., Chen, K.-W., Chai, C.-Y., Chen, W.-T., Fang, A.-H., Chen, Y.-H., and Wu, C.-S. (2016). Heat-killed and live Lactobacillus reuteri GMNL-263 exhibit similar effects on improving metabolic functions in high-fat diet-induced obese rats. Food Funct. *7*, 2374–2388.
27. Zhang, Z., Zhou, Z., Li, Y., Zhou, L., Ding, Q., and Xu, L. (2016). Isolated exopolysaccharides from Lactobacillus rhamnosus GG alleviated adipogenesis mediated by TLR2 in mice. Sci. Rep. *6*, 36083.
28. Sun, W., Yu, Z., Yang, S., Jiang, C., Kou, Y., Xiao, L., Tang, S., and Zhu, T. (2020). A transcriptomic analysis reveals novel patterns of gene expression during 3T3-L1 adipocyte differentiation. Front. Mol. Biosci. *7*, 564339.
29. Gregoire, F.M., Smas, C.M., and Sul, H.S. (1998). Understanding adipocyte differentiation. Physiol. Rev. *78*, 783–809.
30. Ge, S.X., Jung, D., and Yao, R. (2020). ShinyGO: a graphical gene-set enrichment tool for animals and plants. Bioinformatics *36*, 2628–2629.
31. Lee, J.S., Song, W.S., Lim, J.W., Choi, T.R., Jo, S.H., Jeon, H.J., Kwon, J.E., Park, J.H., Kim, Y.R., Yang, Y.H., et al. (2022). An integrative multiomics approach to characterize anti-adipogenic and anti-lipogenic effects of Akkermansia muciniphila in adipocytes. Biotechnol. J. *17*, 2100397.
32. Sanders, M.E., Benson, A., Lebeer, S., Merenstein, D.J., and Klaenhammer, T.R. (2018). Shared mechanisms among probiotic taxa: implications for general probiotic claims. Curr. Opin. Biotechnol. *49*, 207–216.
33. Szklarczyk, D., Kirsch, R., Koutrouli, M., Nastou, K., Mehryary, F., Hachilif, R., Gable, A.L., Fang, T., Doncheva, N.T., Pyysalo, S., et al. (2023). The STRING database in 2023: protein–protein association networks and functional enrichment analyses for any sequenced genome of interest. Nucleic Acids Res. *51*, D638–D646.
34. Si, Y., Yoon, J., and Lee, K. (2007). Flux profile and modularity analysis of time-dependent metabolic changes of *de novo* adipocyte formation. Am. J. Physiol. Endocrinol. Metab. *292*, E1637–E1646.
35. Green, C.R., Wallace, M., Divakaruni, A.S., Phillips, S.A., Murphy, A.N., Ciaraldi, T.P., and Metallo, C.M. (2016). Branched-chain amino acid catabolism fuels adipocyte differentiation and lipogenesis. Nat. Chem. Biol. *12*, 15–21.
36. Zaganjor, E., Yoon, H., Spinelli, J.B., Nunn, E.R., Laurent, G., Keskinidis, P., Sivaloganathan, S., Joshi, S., Notarangelo, G., Mulei, S., et al. (2021). SIRT4 is an early regulator of branched-chain amino acid catabolism that promotes adipogenesis. Cell Rep. *36*, 109345.
37. Liu, K., and Czaja, M. (2013). Regulation of lipid stores and metabolism by lipophagy. Cell Death Differ. *20*, 3–11.
38. Grabner, G.F., Xie, H., Schweiger, M., and Zechner, R. (2021). Lipolysis: cellular mechanisms for lipid mobilization from fat stores. Nat. Metab. *3*, 1445–1465.
39. Homan, E.A., Kim, Y.-G., Cardia, J.P., and Saghatelian, A. (2011). Monoalkylglycerol ether lipids promote adipogenesis. J. Am. Chem. Soc. *133*, 5178–5181.
40. Crown, S.B., Marze, N., and Antoniewicz, M.R. (2015). Catabolism of branched chain amino acids contributes significantly to synthesis of odd-chain and even-chain fatty acids in 3T3-L1 adipocytes. PLoS One *10*, e0145850.
41. Ma, C., Liu, Y., Liu, S., Lévesque, C.L., Zhao, F., Yin, J., and Dong, B. (2020). Branched chain amino acids alter fatty acid profile in colostrum of sows fed a high fat diet. J. Anim. Sci. Biotechnol. *11*, 9.
42. Tormos, K.V., Anso, E., Hamanaka, R.B., Eisenbart, J., Joseph, J., Kalyanaraman, B., and Chandel, N.S. (2011). Mitochondrial complex III ROS regulate adipocyte differentiation. Cell Metab. *14*, 537–544.
43. Lee, J.H., Park, A., Oh, K.-J., Lee, S.C., Kim, W.K., and Bae, K.-H. (2019). The role of adipose tissue mitochondria: regulation of mitochondrial function for the treatment of metabolic diseases. Int. J. Mol. Sci. *20*, 4924.
44. Guntur, A.R., Gerencser, A.A., Le, P.T., DeMambro, V.E., Bornstein, S.A., Mookerjee, S.A., Maridas, D.E., Clemmons, D.E., Brand, M.D., and Rosen, C.J. (2018). Osteoblast-like MC3T3-E1 cells prefer glycolysis for ATP production but adipocyte-like 3T3-L1 cells prefer oxidative phosphorylation. J. Bone Miner. Res. *33*, 1052–1065.
45. Rogatzki, M.J., Ferguson, B.S., Goodwin, M.L., and Gladden, L.B. (2015). Lactate is always the end product of glycolysis. Front. Neurosci. *9*, 22.
46. Liberti, M.V., and Locasale, J.W. (2016). The Warburg effect: how does it benefit cancer cells? Trends Biochem. Sci. *41*, 211–218.
47. Wang, J., Liu, Y., Lian, K., Shentu, X., Fang, J., Shao, J., Chen, M., Wang, Y., Zhou, M., and Sun, H. (2019). BCAA catabolic defect alters glucose metabolism in lean mice. Front. Physiol. *10*, 1140.
48. El-Hattab, A.W., Emrick, L.T., Craigen, W.J., and Scaglia, F. (2012). Citrulline and arginine utility in treating nitric oxide deficiency in mitochondrial disorders. Mol. Genet. Metab. *107*, 247–252.
49. Lefterova, M.I., Haakonsson, A.K., Lazar, M.A., and Mandrup, S. (2014). PPARγ and the global map of adipogenesis and beyond. Trends Endocrinol. Metab. *25*, 293–302.
50. Tang, Q.-Q., Otto, T.C., and Lane, M.D. (2003). Mitotic clonal expansion: a synchronous process required for adipogenesis. Proc. Natl. Acad. Sci. USA *100*, 44–49.
51. Farmer, S.R. (2006). Transcriptional control of adipocyte formation. Cell Metab. *4*, 263–273.
52. Guo, L., Li, X., and Tang, Q.-Q. (2015). Transcriptional regulation of adipocyte differentiation: a central role for CCAAT/enhancer-binding protein (C/EBP) β. J. Biol. Chem. *290*, 755–761.

53. Oishi, Y., Manabe, I., Tobe, K., Tsushima, K., Shindo, T., Fujiu, K., Nishimura, G., Maemura, K., Yamauchi, T., Kubota, N., et al. (2005). Krüppel-like transcription factor KLF5 is a key regulator of adipocyte differentiation. Cell Metab. *1*, 27–39.

54. García-Niño, W.R., and Zazueta, C. (2021). New insights of Krüppel-like transcription factors in adipogenesis and the role of their regulatory neighbors. Life Sci. *265*, 118763.

55. Biswas, D., Duffley, L., and Pulinilkunnil, T. (2019). Role of branched-chain amino acid–catabolizing enzymes in intertissue signaling, metabolic remodeling, and energy homeostasis. FASEB J. *33*, 8711–8731.

56. Ke, Q., and Costa, M. (2006). Hypoxia-inducible factor-1 (HIF-1). Mol. Pharmacol. *70*, 1469–1480.

57. Lee, S.-H., Golinska, M., and Griffiths, J.R. (2021). HIF-1-independent mechanisms regulating metabolic adaptation in hypoxic cancer cells. Cells *10*, 2371.

58. Cifarelli, V., Beeman, S.C., Smith, G.I., Yoshino, J., Morozov, D., Beals, J.W., Kayser, B.D., Watrous, J.D., Jain, M., Patterson, B.W., and Klein, S. (2020). Decreased adipose tissue oxygenation associates with insulin resistance in individuals with obesity. J. Clin. Invest. *130*, 6688–6699.

59. Oates, E.H., and Antoniewicz, M.R. (2023). 13C-Metabolic flux analysis of 3T3-L1 adipocytes illuminates its core metabolism under hypoxia. Metab. Eng. *76*, 158–166.

60. Griffin, M.J. (2022). On the immunometabolic Role of NF-κB in Adipocytes. Immunometabolism *4*, e220003.

61. Kudo, T., Zhao, M.L., Jeknić, S., Kovary, K.M., LaGory, E.L., Covert, M.W., and Teruel, M.N. (2023). Context-dependent regulation of lipid accumulation in adipocytes by a HIF1α-PPARγ feedback network. Cell Syst. *14*, 1074–1086.e7.

62. Mylonis, I., Sembongi, H., Befani, C., Liakos, P., Siniossoglou, S., and Simos, G. (2012). Hypoxia causes triglyceride accumulation by HIF-1-mediated stimulation of lipin 1 expression. J. Cell Sci. *125*, 3485–3493.

63. Kihira, Y., Fujimura, Y., Tomita, S., Tamaki, T., and Sato, E. (2020). Hypoxia-inducible factor-1α regulates Lipin1 differently in pre-adipocytes and mature adipocytes. Mol. Med. Rep. *22*, 559–565.

64. Li, H., Cheng, Y., Wu, W., Liu, Y., Wei, N., Feng, X., Xie, Z., and Feng, Y. (2014). SRSF10 regulates alternative splicing and is required for adipocyte differentiation. Mol. Cell Biol. *34*, 2198–2207.

65. Tyanova, S., Temu, T., and Cox, J. (2016). The MaxQuant computational platform for mass spectrometry-based shotgun proteomics. Nat. Protoc. *11*, 2301–2319.

66. Tyanova, S., Temu, T., Sinitcyn, P., Carlson, A., Hein, M.Y., Geiger, T., Mann, M., and Cox, J. (2016). The Perseus computational platform for comprehensive analysis of (prote) omics data. Nat. Methods *13*, 731–740.

67. Pang, Z., Chong, J., Zhou, G., de Lima Morais, D.A., Chang, L., Barrette, M., Gauthier, C., Jacques, P.É., Li, S., and Xia, J. (2021). MetaboAnalyst 5.0: narrowing the gap between raw spectra and functional insights. Nucleic Acids Res. *49*, W388–W396.

68. Rivière, A., Gagnon, M., Weckx, S., Roy, D., and De Vuyst, L. (2015). Mutual cross-feeding interactions between Bifidobacterium longum subsp. longum NCC2705 and Eubacterium rectale ATCC 33656 explain the bifidogenic and butyrogenic effects of arabinoxylan oligosaccharides. Appl. Environ. Microbiol. *81*, 7767–7781.

69. Wiśniewski, J.R. (2016). Quantitative evaluation of filter aided sample preparation (FASP) and multienzyme digestion FASP protocols. Anal. Chem. *88*, 5438–5443.

70. Folch, J., Lees, M., and Sloane Stanley, G.H. (1957). A simple method for the isolation and purification of total lipids from animal tissues. J. Biol. Chem. *226*, 497–509.

STAR★METHODS

KEY RESOURCES TABLE

REAGENT or RESOURCE	SOURCE	IDENTIFIER
Bacterial and virus strains		
Lactobacillus acidophilus	Korean Collection for Type Cultures	KCTC 3140
Lactobacillus casei	Korean Collection for Type Cultures	KCTC 3109
Lactobacillus fermentum	Korean Collection for Type Cultures	KCTC 3112
Lactobacillus gasseri	Korean Collection for Type Cultures	KCTC 3163
Lactobacillus johnsonii	Korean Collection for Type Cultures	KCTC 3801
Lactobacillus reuteri	Korean Collection for Type Cultures	KCTC 3594
Lactobacillus rhamnosus GG	Korean Collection for Type Cultures	KCTC 5033
Lactobacillus plantarum subsp. plantarum	Korean Collection for Type Cultures	KCTC 3108
Bifidobacterium adolescentis	Korean Collection for Type Cultures	KCTC 3216
Bifidobacterium animalis subsp. animalis	Korean Collection for Type Cultures	KCTC 3219
Bifidobacterium bifidum	Korean Collection for Type Cultures	KCTC 3202
Bifidobacterium breve	Korean Collection for Type Cultures	KCTC 3419
Bifidobacterium infantis	Korean Collection for Type Cultures	KCTC 3249
Bifidobacterium animalis subsp. lactis	Korean Collection for Type Cultures	KCTC 5854
Bifidobacterium longum	Korean Collection for Type Cultures	KCTC 3128
Chemicals, peptides, and recombinant proteins		
Dulbecco's Modified Eagle Medium (DMEM)	Gibco	Cat#10564011
Bovine serum	Gibco	Cat#16170060
Penicillin–streptomycin	Biowest	Cat#L0022
Fetal bovine serum	Biowest	Cat#S1480
3-Isobutyl-1-methylxanthine (IBMX)	Sigma-Aldrich	Cat#I7018
Dexamethasone	Sigma-Aldrich	Cat#D4092
Insulin	Sigma-Aldrich	Cat#I0516
Trypsin/EDTA	Biowest	Cat#L0931
Protease inhibitor cocktail	Sigma-Aldrich	Cat#P8340
Trypsin protease	Thermo Fisher Scientific	Cat#90057
L-Phenylalanine-$^{13}C_9$,^{15}N	Sigma-Aldrich	Cat#608017
Critical commercial assays		
RNeasy Mini Kit	Qiagen	Cat#74104
QIA shredder	Qiagen	Cat#79654
RNase-free DNase kit	Qiagen	Cat#79254
iScript cDNA Synthesis Kit	Bio-Rad	Cat#1708890
SsoAdvanced™ Universal SYBR® Green Supermix	Bio-Rad	Cat#1725271
Deposited data		
Mass spectrometry proteomics data of adipocyte	ProteomeXchange Consortium via the PRIDE	PRIDE: PXD050884
Mass spectrometry metabolomics data of adipocyte	MetaboLights database	Metabolight: MTBLS12185
Experimental models: Cell lines		
3T3-L1	Korean Cell Line Bank	KCLB No.10092.1; RRID: CVCL_0123
Oligonucleotides		
Primer sequences used for qRT-PCR	Table S4	N/A
Software and algorithms		
MaxQuant v1.6.5.0	Tyanova et al.[65]	https://maxquant.net/maxquant/
R studio	R Studio	https://posit.co/products/open-source/rstudio/

(*Continued on next page*)

Continued

REAGENT or RESOURCE	SOURCE	IDENTIFIER
Perseus v1.6.15.0	Tyanova et al.[66]	https://maxquant.net/perseus/
STRING database analysis tool	Szklarczyk et al.[33]	https://string-db.org/
ShinyGO 0.80	Ge et al.[30]	http://bioinformatics.sdstate.edu/go/
MetaboAnalyst 5.0	Pang et al.[67]	https://genap.metaboanalyst.ca/

EXPERIMENTAL MODEL AND STUDY PARTICIPANT DETAILS

Bacterial strains and growth conditions

The bacterial strains used in this study, including *Lactobacillus spp.* and *Bifidobacterium spp.*, were distributed from the Korean Collection for Type Cultures. All bacterial strains used in the experiment were listed in key resources table. *Lactobacillus* strains were cultured in De Man–Rogosa–Sharpe (MRS) agar and *Bifidobacterium* strains in reinforced clostridial medium agar for 3 days at 37°C under anaerobic conditions (90% N_2, 5% CO_2, and 5% H_2). Subsequently, each bacterial strain that produced colonies after agar culture was cultured by inoculating a verified single colony into Media of Colon Bacteria (MCB) broth.[68] All bacterial strains were cultured to the stationary phase and then used in the experiment (Figure S7).

3T3-L1 cell culture and differentiation

The 3T3-L1 cells (KCLB No.10092.1; RRID: CVCL_0123) used in the experiments were obtained from the KCLB. The cell lines were tested for mycoplasma contamination prior to the experiment to ensure clear cells were used. 3T3-L1 preadipocytes were cultured in a CO_2 incubator (37°C, 5% CO_2) and maintained in high glucose Dulbecco's Modified Eagle Medium (DMEM; 10564011, Gibco, MA, USA) containing 10% bovine serum (16170060, Gibco, CA, USA) and 1% penicillin–streptomycin (P/S; L0022, Biowest, USA). Once the cells reached confluence, they were replaced with fresh medium and incubated after confluence for 2 days. Following termination after confluence, cells were washed with PBS and replaced with DMEM containing 10% fetal bovine serum (FBS; S1480, Biowest, MA, USA) and 1% P/S to induce adipocyte differentiation. For the first 48 h, differentiation was induced by treatment with DMEM (10% FBS, 1% P/S) containing an adipogenic cocktail MDI (0.5 mM of 3-isobutyl-1-methylxanthine (IBMX; I7018, Sigma-Aldrich, MO, USA), 4 μg/mL of dexamethasone (DEX; D4092, Sigma-Aldrich, MO, USA), and 10 μg/mL of insulin (I0516, Sigma-Aldrich, MO, USA)). After the initial induction of differentiation, they were replaced with DMEM (10% FBS, 1% P/S) containing 10 μg/mL of insulin to differentiate for 48 h and then replaced with DMEM (10% FBS, 1% P/S) every 2 days for 4 days to accumulate lipids in adipocytes. 3T3-L1 adipocytes were differentiated for 8 days and then confirmed for lipid accumulation. The adipocytes used in the experiments were differentiated for 8 days, and all experiments used 3T3-L1 cells below passage number 8 or lower.

METHOD DETAILS

Preparation of the probiotic lysate

To obtain the probiotic lysate for treatment on adipocyte, each bacterial strain was lysed using an ultrasonic processor (VC 505, Sonics & Materials, Newtown, USA). The bacterial strains that reached the stationary phase were measured for optical density in 600 nm (OD_{600}) using an ultraviolet-visible (UV-vis) spectrophotometer (Multiskan GO, Thermo Fisher Scientific, MA, USA) before cell harvesting. They were then separated from the culture medium by centrifugation (4,000 rpm for 10 min at 4°C). The separated cell pellets were washed twice with phosphate-buffered saline (PBS; pH 7.4) to remove residual MCB medium. Each cell pellet was resuspended in PBS at a concentration of 1×10^{10} colony-forming unit (CFU)/mL. CFU in the cell pellet was calculated from the measured OD_{600} (Figure S8). The cell suspension was lysed using an ultrasonic processor in 1-mL volume, and the condition of lysis was optimized by bicinchoninic acid (BCA) assay (Figure S9). The CFE was obtained by centrifuging the lysate at 13,500 rpm for 5 min at 4°C and filtering the separated supernatant through a 0.45-μm polyvinylidene Fluoride (PVDF) syringe filter. The obtained lysate was diluted with PBS and treated with adipocyte medium at a concentration of 5% (v/v).

Cytotoxicity assay

To confirm the cytotoxicity of the cell lysates to 3T3-L1 cells, cell viability was assessed in mature adipocytes cotreated with each cell lysate for 8 days of differentiation. Culture medium was removed from 3T3-L1 cells on day 8 of differentiation, washed with PBS to remove any remaining residue, and replaced with DMEM (10% FBS, 1% P/S) containing 0.5 mg/mL of methyl thiazolyl diphenyl-tetrazolium bromide (MTT; M5655, Sigma-Aldrich, MO, USA). 3T3-L1 cells were incubated in a CO_2 incubator (37°C, 5% CO_2) for 4 h. After 4 h, the culture medium was removed, and the resulting formazan was lysed in the dark by treatment with lysis buffer containing dimethylformamide/water (1:1 v/v, pH 4.7) with 20 wt% sodium dodecyl sulfate (SDS, 71725, Sigma-Aldrich, MO, USA). Furthermore, formazan dissolved in the lysis buffer was measured for absorbance at 570 nm using a UV-vis spectrophotometer.

Oil Red O staining assay

Lipid droplets produced during adipocyte differentiation were measured using Oil Red O (ORO) staining. Adipocytes were rinsed with PBS to remove any remaining residue and subsequently fixed in a 4% formaldehyde solution (252549, Sigma-Aldrich, MO, USA) for 1 h. The fixed cells were washed with PBS and then treated thrice with 60% 2-propanol (IPA; 34863, Sigma-Aldrich, MO, USA) for 5 min each time. To prepare for ORO staining, any residual IPA was completely removed by drying at 60°C. The dried cells were incubated in a 0.3% ORO solution (3:2 (v/v) mixture of ORO solution and water) for 1 h. The 0.3% ORO solution was prepared by centrifuging and filtering the solution. After incubation, the cells were washed thrice with water for 5 min each. The residue was thoroughly dried at 60°C and treated with 100% IPA to dissolve the stained ORO. The dissolved ORO solution was measured for absorbance at 510 nm using a UV-vis spectrophotometer.

Quantitative real-time PCR

3T3-L1 cells were washed with PBS and then treated with trypsin/EDTA (L0931, 0.25% w/v, Biowest, USA) to obtain cells. The obtained cells were centrifuged at 1000 rpm for 5 min to remove the supernatant and then dissolved in RLT buffer containing 2% β-mercaptoethanol. Cells were homogenized using a QIAshredder spin column (79654, Qiagen, Hilden, Germany) before RNA extraction. Total RNA was prepared using the RNeasy Mini kit (74104, Qiagen, Hilden, Germany), and DNA was removed using the RNase-free DNase kit (79254, Qiagen, Hilden, Germany). The concentration and purity of the extracted RNA were evaluated using a μDrop Plate of UV-vis spectrophotometer. The extracted RNA was synthesized into complementary DNA (cDNA) using the iScript cDNA Synthesis Kit (1708890, Bio-Rad, CA, USA). The primers used in the experiments are shown in Table S4.

The mRNA expression by real-time PCR was measured using CFX Connect™ (Bio-Rad, CA, USA) instrument with SsoAdvanced™ Universal SYBR® Green Supermix (1725271, Bio-Rad, CA, USA). Real-time PCR analysis conditions were performed as follows: 1) polymerase activation and cDNA denaturation at 95°C for 30 s for one cycle only; 2) cDNA denaturation at 95°C for 15 s; 3) annealing and extension at 60°C for 30 s; and 3) repeat denaturation–annealing and extension for 39 cycles. The measured mRNA expression was normalized to β-actin (reference gene).

Proteomic sample preparation and analysis

3T3-L1 cells were washed with PBS to remove the residual medium, then treated with the radioimmunoprecipitation assay (RIPA) buffer (89901, Thermo Fisher Scientific, MA, USA) containing 0.1% (v/v) protease inhibitor cocktail (P8340, Sigma-Aldrich, MO, USA) and cells were harvested using a cell scraper. The obtained cells were completely lysed using an ultrasonic processor. Immediately after cell lysis, the samples were incubated for 25 min at 4°C and then centrifuged to obtain supernatants. The protein concentration of obtained samples was determined using a BCA protein assay kit (23225, Thermo Fisher Scientific, Pittsburgh, USA). Protein samples were prepared via a modified filter-aided sample preparation method.[69] The samples were reduced at 95°C for 5 min by adding 1-M dithiothreitol (DTT; 43815, Sigma-Aldrich, MO, USA) to make a final concentration of 50 mM. After the reaction was terminated, 200 μg of protein was loaded on a Microcon 30 kDA filter unit (MRCF0R030, Merck Millipore, Darmstadt, Germany) and UA buffer (8 M urea in 0.1 M Tris/HCl, pH 8.5) was added to bring the volume to final 500 μL. The filter unit was centrifugated twice (13,500 rpm for 15 min), and then 200 μL of UA buffer was added to the filter and centrifugated twice under the same conditions. Subsequently, 100 μL of UA buffer containing 50 mM of iodoacetamide (IAA; I1149, Sigma-Aldrich, MO, USA) was added to the filter unit and incubated for 20 min in the dark. Then, the filter unit was centrifugated twice (13,500 rpm for 10 and 15 min) with 100 μL of UA buffer. Furthermore, 100 μL of Tris/HCl buffer (0.05 M) was added to the filter and centrifuged (13,500 rpm for 10 min) twice, and this process was repeated twice. Finally, 2 μg of trypsin protease (90057, Thermo Fisher Scientific, MA, USA) dissolved in 0.05 M Tris/HCl buffer was added to the filter to ensure 1:100 trypsin/protein (w/w) and incubated overnight at 37°C. After the reaction, the samples were eluted by adding 0.05 M of Tris/HCl buffer and then centrifuged (13,500 rpm for 10 min). The eluted samples were purified using Pierce Peptide Desalting Spin Columns (89851, Thermo Fisher Scientific, MA, USA) according to the manufacturer's protocol. The purified samples were dried using a centrifugal vacuum concentrator (Hanil Scientific Inc., Korea) and stored at −80°C until use.

Dried samples were dissolved in a water/acetonitrile (98:2 (v/v)) solution supplemented with 0.1% formic acid, and the protein concentration was measured by BCA assay. Based on the measured protein concentration, all samples were diluted to a concentration of 1 μg/mL. The sample injection into the instrument was 2 μg, and separation was performed using a mixture of solvent A (water/acetonitrile (98:2 v/v) solution containing 0.1% formic acid) and solvent B (100% acetonitrile containing 0.1% formic acid). The injected sample was first trapped on an Acclaim PepMap 100 trap column (100 μm × 2 cm, nanoViper C18, 5 μm, 100 Å, Thermo Scientific, part number 164564) and washed with 98% A for 6 min at a flow rate of 4 μL/min. They were then separated on an Acclaim PepMap 100 capillary column (75 μm × 15 cm, nanoViper C18, 3 μm, 100 Å, Thermo Scientific, part number 164568) at a flow rate of 300 nL/min with an electrospray voltage setting of 2.1 kV. The gradient conditions of the LC solution were 0 min, 2% B; 45 min, 2%–40% B; 5 min, 40%–95% B; 10 min, 95% B; and 20 min 2% B. Samples were analyzed by a Q Exactive Hybrid Quadrupole-Orbitrap mass spectrometer (Thermo Scientific, USA) and an Orbitrap Exploris 240 mass spectrometer (Thermo Scientific, USA) coupled to a Dionex Ultimate 3000 RSLCnano high-performance liquid chromatography (HPLC) system (Thermo Scientific, MA, USA). Analyzed data were collected automatically using Proteome Discoverer 2.5 (Thermo Scientific, USA). The Orbitrap analyzer scanned precursor ions with a mass range of 350–1800 m/z with a resolution of 70,000 and 60,000 at m/z 200, respectively. Protein identification and quantification were processed against *Mus musculus* (UniProt ID: UP000000589) database using MaxQuant (version 1.6.5.0), and the results were quantified by label-free quantification (LFQ).[65] The retrieved proteins were processed using Perseus 1.6.15.0.[66]

Metabolomics sample preparation and analysis

3T3-L1 cells were washed with PBS twice to remove the residual medium. Cells were quickly treated with 500 μL of cold 80% methanol (99.99%, HPLC grade, Honeywell, B&J) containing 10 μm of L-Phenylalanine-$^{13}C_9$,^{15}N (608017, Sigma-Aldrich, MO, USA) as an internal standard and then quenched at −80°C for 20 min. Quenched cells were harvested using cell scrapers and transferred to cold tubes. All metabolite extraction experiments were performed on ice. The harvested cells were strongly vortexed for 10 s and centrifuged (13,500 rpm for 20 min at 4°C). The centrifuged supernatant was obtained and dried using a centrifugal vacuum concentrator. Intracellular metabolite extraction samples were stored at −80°C until use. The remaining cell pellet was washed with 100% methanol and dissolved in the RIPA buffer to measure protein concentration, which was used to normalize the metabolite analysis results.

Dried samples were dissolved in HPLC water (W5-4; Fisher) and filtered through a 0.45-μm PVDF syringe filter. Filtered samples were transferred to LC-certified vials (Agilent, USA) and analyzed by LC–MS system combining triple-quadrupole mass spectrometry (QQQ; 6420 Triple Quadrupole, Agilent, USA) and HPLC (1260 Infinity Binary LC, Agilent, USA). Metabolites were separated via an X-bridge amide column (4.6 x 100 mm, 3.5 μm particle size, Waters, Milford, USA) using a mixture of solvent A (water/acetonitrile (95:5 v/v) solution containing 20-mM ammonium acetate and 20-mM ammonium hydroxide) and solvent B (100% acetonitrile). Analytes were separated by an LC solution gradient at a flow rate of 0.4 mL/min with an injection of 10 μL under an electrospray voltage setting of 4 kV. The gradient conditions were 0 min, 85% B; 5 min, 42% B; 16 min, 0% B; 24 min 0% B; 25 min, 85% B; and 32 min, 85% B. The peak area of the detected metabolites was identified using Agilent Mass Hunter Qualitative Analysis, and the peak areas were normalized by the peak areas of the internal standard.

Lipid extraction and mild alkaline methanolysis

3T3-L1 cells were washed with PBS and treated with 600 μL of trypsin to harvest cells, then washed twice with PBS. Lipid was extracted using the Folch method, a commonly used method, with minor modifications.[70] Cells were lysed with 1 mL of cold methanol and transferred to glass vials. Cells were incubated at 4°C for 10 min and then vortexed strongly for 30 s by adding 2 mL of cold chloroform. The cells were incubated again at 4°C for 30 min, vortexing strongly at 10-min intervals. After brief vortexing at the end of the incubation, 1 mL of 0.9% NaCl was added, followed by vortexing for 30 sec and incubation at 4°C for 10 min. The upper phase was removed by centrifugation (4,000 rpm for 20 min at 4°C), and only the lower phase was taken and transferred to new tubes. The transferred samples were dried under compressed nitrogen and stored at −80°C until use.

Dried samples were dissolved in toluene/methanol (toluene/methanol = 1:1 (v/v)) and then 0.2-M KOH/methanol was added. The samples were incubated at 37°C for 15 min for derivatization using mild alkaline methanolysis. Distilled water, 1 M acetic acid solution (695092, Sigma-Aldrich, MO, USA), and hexane (34859, Sigma-Aldrich, MO, USA) were added to the samples and vortexed. The upper phase was collected by centrifugation, and the hexane was evaporated using a nitrogen evaporator (EYELA, Singapore) to avoid oxidation. Chloroform containing 100-μg/mL methyl heneicosanoic acid, an internal standard, was added to the dried sample and filtered through a 0.22-μm PVDF syringe filter. Fatty acids were analyzed using a GC-MS system (Clarus 500, PerkinElmer, USA). Then, 1 μL of the prepared analytical sample was injected into the instrument and separated by temperature gradient using an Elite-5ms capillary column (30 m × 0.25 mm × 0.25 μm; Perkin Elmer, USA) at a flow rate of 1 mL/min with helium as mobile phase. The gradient conditions were hold at 120°C for 5 min; increase to 200°C at a rate of 6°C/min; increase to 220°C at a rate of 2°C/min; increase to 300°C at a rate of 10°C/min and hold for 10 min. The injector, inlet line, and source temperatures were set to 280°C, 280°C, and 250°C, respectively, and the MS spectrum was set to 45–400 mass-to-charge ratio (m/z). The detected fatty acids were quantified via a standard concentration curve (g/L) versus intensity.

QUANTIFICATION AND STATISTICAL ANALYSIS

Statistical analysis

Statistical analysis was performed using R statistical environment, Perseus, and MetaboAnalyst 5.0.[67] Data were represented as the mean ± SD. All data were normalized with the mean of control, and significant differences between the two groups were assessed to the unpaired two-tailed Student's T-test. Significant differences between three or more groups were analyzed using one-way analysis of variance (ANOVA) followed by post hoc Tukey's honestly significant difference (HSD) test. Statistical comparison was indicated with *, **, and *** for $p < 0.05$, $p < 0.01$, and $p < 0.001$, respectively.